

DYNAMIC SIR/SEIR-LIKE MODELS COMPRISING A TIME-DEPENDENT TRANSMISSION RATE: HAMILTONIAN MONTE CARLO APPROACH WITH APPLICATIONS TO COVID-19

Hristo Inouzhe Valdes¹, María Xosé Rodríguez-Álvarez^{2,3}, Lorenzo Nagar¹, and Elena Akhmatskaya^{1,4}

¹*BCAM, Basque Center For Applied Mathematics, Bilbao, Spain.*

²*CINBIO, Universidade de Vigo, Department of Statistics and Operations Research, Vigo, Spain.*

³*CITMAga, Galician Center for Mathematical Research and Technology, Santiago de Compostela, Spain*

⁴*IKERBASQUE, Basque Foundation for Science, Bilbao, Spain*

January 18, 2023

Abstract

A study of changes in the transmission of a disease, in particular, a new disease like COVID-19, requires very flexible models which can capture, among others, the effects of non-pharmacological and pharmacological measures, changes in population behaviour and random events. In this work, we give priority to data-driven approaches and choose to avoid a priori and ad-hoc methods. We introduce a generalised family of epidemiologically informed mechanistic models, guided by Ordinary Differential Equations and embedded in a probabilistic model. The mechanistic models SI_KR and $SE_M I_KR$ with K Infectious and M Exposed sub-compartments (*resulting in non-exponential infectious and exposed periods*) are enriched with a time-dependent transmission rate, parametrized using Bayesian P-splines. This enables an extensive flexibility in the transmission dynamics, with no ad-hoc intervention, while maintaining good differentiability properties. Our probabilistic model relies on the solutions of the mechanistic model and benefits from access to the information about under-reporting of new infected cases, a crucial property when studying diseases with a large fraction of asymptomatic infections. Such a model can be efficiently differentiated, which facilitates the use of Hamiltonian Monte Carlo for sampling from the posterior distribution of the model parameters. The features and advantages of the proposed approach are demonstrated through comparison with state-of-the-art methods using a synthetic dataset. Furthermore, we successfully apply our methodology to the study of the transmission dynamics of COVID-19 in the Basque Country (Spain) for almost a year, from mid February 2020 to the end of January 2021.

1 Introduction

COVID-19 is ‘a mild to severe respiratory illness that is caused by a coronavirus (Severe Acute Respiratory Syndrome Coronavirus 2 (SARS-COV-2) of the genus Betacoronavirus), and it is characterised especially by fever, cough, and shortness of breath and may progress to pneumonia and respiratory failure’ (Merriam-Webster dictionary). The global spread of this new coronavirus reached the status of a pandemic, by the criteria of the World Health Organization (WHO), on the 11th of March 2020. The impact of the COVID-19 pandemic has been devastating in many aspects of human existence. At the moment of writing, more than 6.6 million lives have been lost (see John Hopkins Coronavirus Resource Center at <https://coronavirus.jhu.edu/map.html>). This terrible death toll has been accompanied by severe social and economic crises (see, e.g. [42]). In the context of emergency, it is not surprising that, during the period 2020-2022, the scientific community has focused its attention on different aspects of SARS-COV-2.

To help with decision making and to minimise adverse consequences of the pandemic, the mathematical community has been putting enormous effort into designing models that describe how COVID-19 spreads in a population and what are the consequences of this spread, e.g. hospitalisation, mortality, etc. The task is greatly facilitated by methods that had been already developed for other diseases such as influenza, AIDS, malaria, SARS, Ebola, dengue [4, 24], but remains a difficult challenge. Focusing mainly on COVID-19 related research, and following [12, 45, 46], we can split modelling approaches into four general groups:

- *Mechanistic*: the disease dynamics is purely governed by differential equations which are usually epidemiologically motivated [3, 8, 17, 30, 37, 38, 40, 56]
- *Statistical*: a statistical model is fitted to disease related data, such as daily cases, mortality, and so on, without necessarily using epidemiological insights. Relevant methods are Generalized Linear Models (GLMs), time series, stochastic processes, etc. [6, 9, 14, 47, 54, 55]
- *Agent Based Models*: the affected population is modelled as a network of interacting individuals [18]
- *Dynamic models*: mechanistic models embedded in probabilistic models [1, 16, 17, 19, 21, 32, 34, 36, 51, 53, 58]

The amount of models developed for COVID-19 is overwhelming, and currently more are being developed. Therefore, we do not claim that the previously cited studies are a complete overview of the topic.

Our focus through this work is on dynamic models. We aim at epidemiologically informed mechanistic models able to partially describe the complex reality of COVID-19 (as well as other infectious diseases) transmission and to utilise available data for estimating (some of) the unknown parameters governing such models. This will be done through the introduction, on top of a mechanistic model, of probabilistic/generative models to make efficient use of the observed (and noisy) data. In particular, the parameters’ estimation will be done within the Bayesian paradigm, which allows to naturally incorporate prior knowledge on the parameters of the mechanistic model and to quantify the uncertainty of the results in a consistent and coherent way.

The most widely used mechanistic models, and therefore, the base of many dynamic models, are compartmental models. Compartmental models work by splitting the population into disjoint compartments, then proposing a flow diagram between compartments, see Figure 1, and, finally, codifying this flow diagram into an Ordinary Differential Equation (ODE) system that governs

the transmission process of the disease (see [37]). The best-known compartmental models are the Susceptible-Infectious-Removed (SIR), introduced in [29], and the Susceptible-Exposed-Infectious-Removed (SEIR) models. Generalisations of these models, introducing a more realistic distribution of the time spent in the exposed and infectious compartments, were discussed in [2, 5, 39]. We will denote them as SI_KR and $SE_M I_KR$, with K (M) standing for the split of the infectious (exposed) compartment into K (M) sub-compartments. In SIR and SEIR-like models, the driving force of the disease transmission is usually modelled by the transmission rate (denoted by β), i.e., the average number of contacts per person per time unit multiplied by the probability of infection in a contact. Thus, the transmission rate guides the transition from the susceptible to the infectious or exposed compartments, respectively. A related quantity is the basic reproduction number (R_0), which is the expected number of new infected cases generated by a single infected person.

Typically, the transmission rate is assumed to be a constant. However, this may be too restrictive and non-realistic, especially for COVID-19, as one expects changes in the transmission in response to different factors. On the one hand, changes may be due to non-pharmacological measures such as mask requirements, lockdowns, curfews, capacity restrictions, and so on. On the other hand, changes may come from alterations in group behaviour due to more knowledge, weariness, panic, etc. Alternatively, pharmacological measures as vaccines are usually taken into account by explicit extensions to SIR and SEIR-like models but their effect can also be captured by a time-dependent transmission rate. Non-pharmacological measures usually aim at reducing contact between people, or at lowering the probability of getting infected when a contact occurs, or at both. Hence, their purpose is to slow down the spread of the disease, which can be modelled as a reduction in the transmission rate in SIR and SEIR-like models. In contrast, weariness or irresponsible behaviour at the population level can result in an acceleration of the spread of the disease, which can be modelled as an increase in the transmission rate. In a raging pandemic caused by a new disease, as is the case for COVID-19, changes in group behaviour are frequent, and diverse non-pharmacological measures are adopted at different points in time. Hence, when using SIR and SEIR-like models it is justified to require the use of a time-dependent transmission rate instead of a constant one. Even more, the time-dependent transmission rate should be flexible enough to capture this variability.

In this work, we propose to enrich compartmental models with a flexible time-dependent transmission rate, parameterized using P-splines ([35]). The use of P-splines provides extensive flexibility in the transmission dynamics and avoids the need for ad-hoc or parametric specifications of the transmission rate. Reduced to its core, the problem one faces is the determination of parameters values of a compartmental model (as well as of the P-spline) that are compatible with an available dataset. The simplest idea would be to pick a compartmental model of our preference (e.g. the above mentioned SI_KR and $SE_M I_KR$ models) and to fit it to the raw data, obtaining a point estimate of the best parameters. Although potentially very useful ([8]), a point estimate of the model parameters is insufficient due to the limited quantification of the confidence in such an estimate, which is caused by uncertainty in both the data and model parameters. Uncertainty in the data may come from measurement errors, random events during the transmission process, lack of knowledge or capability for precise measurements, etc. Uncertainty in the model parameters refers to the fact that often a range of parameter values, instead of a single combination, is compatible with the available data. Considering the diverse sources of uncertainty is a crucial task in modelling disease transmission as pointed out in [57]. Hence, to account for uncertainty in the data we use a probabilistic model based on the compartmental model and resort to the Bayesian paradigm for the parameters' estimation. Bayesian methods have shown to be well suited for the epidemiological context (see for example [13, 57]).

In this way, we can present a range of plausible parameters for a model based on noisy data and

informed by some prior knowledge. Moreover, we make use of Hamiltonian Monte Carlo (HMC) methods to obtain a sample of the posterior distribution of the parameters. HMC makes use of Hamiltonian dynamics and of the gradient of the log-posterior to propose candidates in a Markov chain. Its main advantages are its avoidance of random walk behaviour when properly tuned, and a better convergence and performance for high-dimensional problems compared to other Markov Chain Monte Carlo (MCMC) methods. The combination of these advantages can result in an additional gain in efficiency (see section 5.3.3 in [44]). To the best of our knowledge, HMC methods have not been used in dynamic models when the transmission rate or the basic reproduction number is time-dependent and belongs to a wide space of functions (for a time-dependent logistic shape see [23]; for a time-independent case see, for example [10]).

Our main contributions in this work are the following. 1) Inspired by [20, 22, 26] we enrich SI_KR and $SE_M I_K R$ models with a time-dependent transmission rate parametrized using Bayesian P-splines ([35]). Hence, we provide well known and widely successful compartmental models with a time-dependent transmission rate in a functional space capable of capturing a wide range of transmission patterns. 2) We propose a dynamic model based on these compartmental models in order to handle uncertainty in the data. 3) We enable an HMC sampling from the parameters' posterior distribution through explicit and semi-analytical calculation of the involved gradients. 4) We provide a means for realisation of our approach which relies on the tools developed in [50]. 5) We supply a synthetic dataset and use it for validation of the proposed methodology through comparison with the corresponding diffusion-based models utilizing well-established SMC² sampler ([11]). 6) Finally, we apply our methods to estimate the transmission behaviour of the COVID-19 pandemic in the Basque Country in Spain.

The structure of this paper is the following. The proposed modelling framework is detailed in Methods. First, we introduce the mechanistic models $SE_M I_K R$ with a spline-based transmission rate. Next, we discuss a Negative Binomial generative probabilistic model based on the solutions of the mechanistic dynamics. The main elements of the suggested Bayesian approach are developed in Bayesian set-up. The summary of the Hamiltonian-based sampling strategy concludes the method section. The synthetic dataset and the COVID-19 daily incidence data of the Basque Country are presented in Data, whereas two case studies built on them are discussed in Results and discussion. We summarise our contributions and future plans in Conclusions. Some technical details and extra results for the two case studies are available as Supplementary Materials.

2 Methods

In this section, we describe in-depth all components of the proposed methodology. This includes a formulation and implementation of (i) a mechanistic dynamic model for the disease transmission and (ii) a probabilistic model incorporating the solutions of the mechanistic dynamics, the data to fit and a Hamiltonian Monte Carlo sampling.

2.1 Mechanistic dynamics

The compartmental models that we choose as a foundation of our models are SI_KR and $SE_M I_K R$, introduced in [2] (with a constant transmission rate β), and their flow diagrams are depicted and explained in Figure 1. These models are extensions of the well-known SIR and SEIR models. For brevity, we omit subindexes when the values of K and M are equal to 1. Splitting the Infected and Exposed compartments imposes an Erlang distribution (a gamma distribution with an integer shape parameter) for the infectious and exposed periods, which is more flexible and usually more

realistic than the exponential distribution assumed by SIR and SEIR models. We remark that, for the models displayed in Figure 1, the average time spent on being exposed is $1/\alpha$ and the average time being infectious is $1/\gamma$. An informative study of the effects of the distribution for the infectious period in these Erlang-based models is presented in [33]. It is important to notice that the split of the compartments does not have to reflect a real distinction in the development of the disease, although it could, but it is rather a mathematical artefact imposing a desired behaviour in the model.

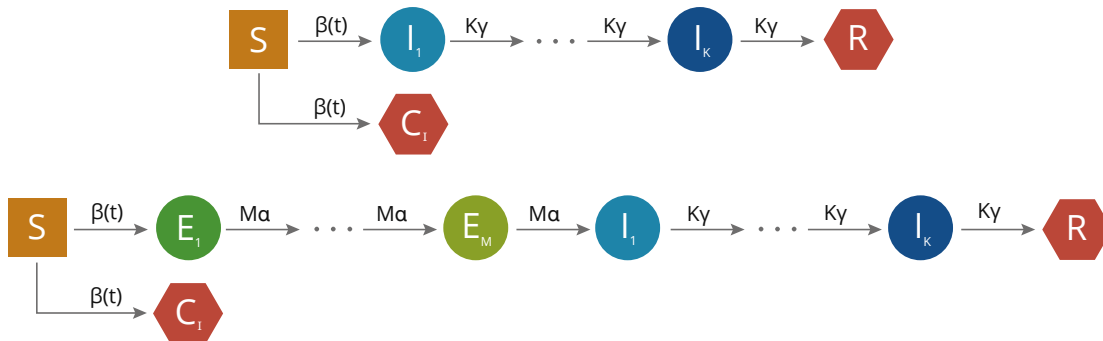


Figure 1: Flow Diagrams for SI_KR (top) and $SE_M I_KR$ (bottom) models with time-dependent transmission rate $\beta(t)$. The S compartment represents the number of individuals in the population susceptible to be infected. The E_1, \dots, E_M compartments reflect the number of individuals at the different stages of exposure, when individuals are infected but are not yet infectious. The I_1, \dots, I_K compartments represent the number of individuals at the different stages of infectiousness, when individuals are infected and infectious. Here $M\alpha$ and $K\gamma$ are constant rates associated with compartments E_i ($i = 1, \dots, M$) and I_j ($j = 1, \dots, K$) respectively. Therefore, the average time spent in an exposed compartment (E_i) is given by $\frac{1}{M\alpha}$, and the average time being exposed is given by $\frac{1}{\alpha}$. Similarly, the average time spent in an infectious compartment (I_j) is given by $\frac{1}{K\gamma}$, and the average time being infectious is given by $\frac{1}{\gamma}$. The R compartment is the number of individuals removed from the pool of susceptible, either dead or recovered with permanent (long lasting) immunity. The time-dependent transmission rate $\beta(t)$ is defined as the average number of contacts per person per time unit multiplied by the probability of infection in a contact between a susceptible and an infected individual. It governs the transition between being susceptible and being infected. The C_I compartment is out of the transmission process and just counts the total number of individuals that have been infected.

To model the time-dependent transmission rate $\beta(t)$, we follow [20, 22, 26] and use splines. In particular, we consider

$$\log \beta(t) = \sum_{i=1}^m \beta_i B_i(t), \quad (1)$$

where functions $\{B_i(t)\}_{i=1}^m$ form a B-spline basis over a time interval $[t_0, t_1]$, with $m = Q + d - 1$, Q the number of (internal) knots and d the degree of the polynomials of the B-splines, and $\boldsymbol{\beta} := (\beta_1, \dots, \beta_m)'$ is a vector of coefficients. For an in-depth discussion on splines, we refer to [15]. Alternative approaches for modelling the time-dependent transmission rate have been proposed, based on, for example, Legendre polynomials as in [51] or diffusion processes as in [16]. However, splines are particularly suitable for our purpose of using HMC methods.

With the previous considerations, the ODE equations corresponding to the $SE_M I_K R$ model, which is represented by the bottom flow diagram in Figure 1, are the following:

$$\begin{aligned}
\frac{dS(t)}{dt} &= -\exp\left(\sum_{i=1}^m \beta_i B_i(t)\right) S(t) \frac{\sum_{j=1}^K I_j(t)}{N} = -\beta(t) S(t) \frac{I(t)}{N}, \\
\frac{dE_1(t)}{dt} &= \exp\left(\sum_{i=1}^m \beta_i B_i(t)\right) S(t) \frac{I(t)}{N} - M\alpha E_1(t), \\
\frac{dE_2(t)}{dt} &= M\alpha E_1(t) - M\alpha E_2(t), \quad \dots \quad , \frac{dE_M(t)}{dt} = M\alpha E_{M-1}(t) - M\alpha E_M(t), \\
\frac{dI_1(t)}{dt} &= M\alpha E_M(t) - K\gamma I_1(t), \\
\frac{dI_2(t)}{dt} &= K\gamma I_1(t) - K\gamma I_2(t), \quad \dots \quad , \frac{dI_K(t)}{dt} = K\gamma I_{K-1}(t) - K\gamma I_K(t), \\
\frac{dR(t)}{dt} &= \frac{d}{dt} (N - S(t) - E(t) - I(t)) = K\gamma I_K(t), \\
\frac{dC_I(t)}{dt} &= \exp\left(\sum_{i=1}^m \beta_i B_i(t)\right) S(t) \frac{I(t)}{N},
\end{aligned} \tag{2}$$

with initial conditions:

$$\begin{aligned}
S(t_0) &= N - E_0, E_1(t_0) = C_I(t_0) = E_0, \\
E_2(t_0) &= \dots = E_M(t_0) = I_1(t_0) = \dots = I_K(t_0) = R(t_0) = 0,
\end{aligned}$$

where $E(t) = \sum_{i=1}^M E_i(t)$, $I(t) = \sum_{j=1}^K I_j(t)$, and $N = S(t) + E(t) + I(t) + R(t)$ is the fixed size of the total population.

This system of ODEs can be interpreted as follows. The change in susceptible population at time t , $dS(t)/dt$, is given by susceptible individuals becoming infected in a way governed by the transmission rate, $\beta(t)$, and proportional to the number of susceptible and infectious individuals, $S(t)$ and $I(t)$ respectively. All newly infected individuals at time t , $\beta(t)S(t)I(t)/N$, go to compartment E_1 while some abandon it at rate $M\alpha$. The individuals that abandoned E_1 at time t , $M\alpha E_1(t)$, go to compartment E_2 , while some abandon E_2 at rate $M\alpha$. This goes on until the individuals that abandon compartment E_M at time t , $M\alpha E_M(t)$, go to I_1 and are now infectious. Individuals abandoning compartment I_1 go to I_2 at rate $K\gamma$. This continues until the last compartment of infectious individuals, I_K , is reached. The ones that abandon it at time t , $K\gamma I_K(t)$, go to the removed compartment, R , which is the final stage of transmission.

A solution of the system (2) provides $S(t), E_1(t), \dots, E_M(t), I_1(t), \dots, I_K(t), R(t)$ for t in a certain time period $[t_0, t_1]$ (typically t_0 is the beginning of the transmission process). That is, the solution provides the number of individuals at each stage (compartment) of the transmission process at a given time t (i.e., it provides prevalent cases). To obtain cumulative (and incident) cases, we introduce in our dynamics a counting compartment C_I . Note that all individuals that become infected at time t , $\beta(t)S(t)I(t)/N$ (i.e., the incidence at time t) are added to compartment C_I but no one leaves it. Thus, $C_I(t)$ represents the total number of infected individuals up to time t . Let t be measured in days and $0 < j < t_1 - t_0$ with $j \in \mathbb{N}$. Then, $C(t_0 + j) = C_I(t_0 + j) - C_I(t_0 + j - 1)$ is the total number of new infected individuals for day j of the disease transmission, i.e., the daily incidence at day j .

The initial conditions are required in order to give a unique solution to the ODE system. Essentially, they mean that at the beginning of the transmission process, t_0 , there were E_0 infected but not infectious individuals, since the latter are accounted in compartment I_1 . This initial scenario makes sense when the first infected individuals are recently exported from a different region to the one of interest.

For ease of notation and brevity, we make the following definition

$$\begin{aligned} \mathbf{y}(t) &= (y_1(t), y_2(t), \dots, y_{M+1}(t), y_{M+2}(t), \dots, y_{M+K+1}(t), y_{M+K+2}(t), y_{M+K+3}(t))' \\ &= (S(t), E_1(t), \dots, E_M, I_1(t), \dots, I_K(t), R(t), C_I(t))'. \end{aligned} \quad (3)$$

where the prime notation $'$ denotes the transpose operation. With this, a condensed form of (2) is given by

$$\dot{\mathbf{y}}(t) = \frac{d\mathbf{y}(t)}{dt} = \mathbf{f}(t, \mathbf{y}, \mathbf{p}), \quad \mathbf{y}(t_0) = (N - E_0, E_0, 0, \dots, 0, E_0)', \quad (4)$$

where $\mathbf{f}(t)$ is the vector formed by the right hand side of the equalities in the ODE system (2) and \mathbf{p} are the parameters of the model (see (6), below). The equations for the SI_KR model are provided in A.

2.2 Probabilistic model

Once the decision on a mechanistic model for the transmission of the disease is made, and the parameters for that model are chosen, one can proceed to the next step.

It is important to remark that in a pandemic, daily incidences, $\{\tilde{C}_{t_0+j}\}_{j=1}^n$, that account for the new daily positive cases for n days, are noisy due to myriad of factors, such as a lack of information, changes in measurement criteria, errors, human behaviour, randomness, etc. A standard way of handling the noise is to use a probabilistic model based on the solutions of a mechanistic one. To follow this idea, we propose to view \tilde{C}_{t_0+j} as a particular realization of a random variable $\tilde{C}(t_0 + j)$ which has the daily incidence at day j , $C(t_0 + j) = C_I(t_0 + j) - C_I(t_0 + j - 1)$, obtained with the help of (2), as its mean value.

Additionally, it is extremely important for COVID-19 modelling to take explicitly into account under-reporting of new infected cases, which arises due to the interplay between insufficient testing and the presence of infectious asymptomatic individuals. The information about under-reporting is usually obtained by seroprevalence studies, see for example [41, 48]. To include under-reporting in the probabilistic model, we use a function $0 < \eta(t) \leq 1$, which provides a fraction of new positive cases that are actually detected, and which should be taken from some external estimation or from expert knowledge. This implies that the actual data to model are not the original $\{\tilde{C}_{t_0+j}\}_{j=1}^n$ but $\{\tilde{C}_{t_0+j}/\eta(t_0 + j)\}_{j=1}^n$. In the absence of under-reporting, $\eta(t) = 1$ for any time t .

In these settings, we propose the probabilistic model that describes new infected cases at time t , $\tilde{C}(t)$, and relies on the solution $C_I(t)$ of the $SE_M I_K R$ equations (2), as follows:

$$\frac{\tilde{C}(t)}{\eta(t)} \sim \text{NegativeBinomial}(C(t) = C_I(t) - C_I(t - 1), \phi), \quad (5)$$

with $\phi > 0$, where

$$P\left(\frac{\tilde{C}(t)}{\eta(t)} = k\right) = \binom{k + \phi - 1}{k} \left(\frac{C(t)}{C(t) + \phi}\right)^k \left(\frac{\phi}{C(t) + \phi}\right)^\phi,$$

and

$$\mathbb{E} \left[\frac{\tilde{C}(t)}{\eta(t)} \right] = C(t) \quad \text{and} \quad \text{Var} \left[\frac{\tilde{C}(t)}{\eta(t)} \right] = C(t) + \frac{C^2(t)}{\phi}.$$

Here, $\phi^{-1} = 1/\phi$ controls the over-dispersion around $C(t)$. The advantages of using a Negative Binomial, which can be viewed as a Poisson distribution with overdispersion, are discussed in [20].

In summary, the proposed probabilistic model $\tilde{C}(t)$ aims to represent the observed data $\{\tilde{C}_{t_0+j}\}_{j=1}^n$ as a down-weighting by $\eta(t)$ of a random variable centered around mechanistic dynamics corrected for under-reporting. Recall that $C(t)$ represents the expected number of new infected individuals at time t , or, in other words, the nearly ‘true’ daily incidence if all newly infected were detected.

2.3 Bayesian set-up

Our next objective is to set up a procedure for estimating parameters of the introduced probabilistic model using the available data. For this purpose, we choose a Bayesian framework. More precisely, our goal is to obtain a posterior distribution of the parameters

$$\mathbf{p} = (p_0, p_1, p_2, p_3, p_4, p_5, \dots, p_{m+4})' = (\alpha, \gamma, E_0, \phi^{-1}, \tau, \boldsymbol{\beta}')', \quad (6)$$

given the observed data $\{\tilde{C}_{t_0+j}\}_{j=1}^n$ and the prior knowledge on these parameters. All parameters in (6) but ϕ^{-1} (it appears in the probabilistic model (5)) are associated with the mechanistic model (2). In the proposed setting, the log-posterior distribution takes the following form:

$$\begin{aligned} \ell(\mathbf{p}) &= \ell_{\text{like}}(\mathbf{p}) + \ell_{\text{prior}}(\mathbf{p}) \\ &= \sum_{j=1}^n \ell_{\text{like}}^j(\mathbf{p}) + \ell_{\text{prior}}(\mathbf{p}) \\ &= \sum_{j=1}^n \log \left(\frac{\Gamma(\frac{\tilde{C}_{t_0+j}}{\eta(t_0+j)} + \phi)}{\Gamma(\phi)\Gamma(\frac{\tilde{C}_{t_0+j}}{\eta(t_0+j)} + 1)} \left(\frac{C(t_0+j)}{C(t_0+j) + \phi} \right)^{\frac{\tilde{C}_{t_0+j}}{\eta(t_0+j)}} \left(\frac{\phi}{C(t_0+j) + \phi} \right)^\phi \right) + \ell_{\text{prior}}(\mathbf{p}). \end{aligned} \quad (7)$$

While the choices of prior distributions for α, γ, E_0 and ϕ^{-1} will be analysed in the context of the studied datasets, here we discuss a prior on coefficients $\boldsymbol{\beta} := (\beta_1, \dots, \beta_m)'$ in (1), i.e., the coefficients associated with the time-dependent transmission rate. In particular, we propose using Bayesian P-splines [35] for that purpose. In brief, in Bayesian P-splines, a moderately large number m of B-spline basis functions associated with equidistant knots is taken (to ensure enough flexibility), and a random walk of order q is used as a prior on $\boldsymbol{\beta}$ to guarantee smoothness. For instance, for a random walk of order 2 one has

$$\beta_i = 2\beta_{i-1} - \beta_{i-2} + u_i = -(i-2)\beta_1 + (i-1)\beta_2 + \sum_{k=3}^i (i+1-k)u_k, \quad i = 3, \dots, m,$$

where $u_i \stackrel{\text{iid}}{\sim} N(0, \tau^2)$ and $P(\beta_0, \beta_1) \propto \text{const.}$ Thus, the joint prior distribution for $\boldsymbol{\beta}$ is a partially improper multivariate Gaussian distribution

$$P(\boldsymbol{\beta} := (\beta_1, \dots, \beta_m)' | \tau^2) \propto \exp \left(-\frac{1}{2\tau^2} \boldsymbol{\beta}' \mathbf{K} \boldsymbol{\beta} \right), \quad (8)$$

for an appropriate matrix \mathbf{K} (the impropriety arises from \mathbf{K} not being of full rank). For an explicit expression for \mathbf{K} see section 4.2.2.1 in [31] (we note that \mathbf{K} depends on q , the order of the random

walk; in this work we will use $q = 2$). As can be seen, the improper prior (8) depends on a single hyper-parameter τ , which controls smoothness. We shall note that, as stated in [20], in (Bayesian) P-splines the number of B-spline basis functions, m , and their degree, d , provided that m is large enough, barely affect the shape of the final estimate that is mainly regulated by the strength of the (roughness) penalty, τ .

To proceed with Bayesian estimation of parameters (6) we propose to use the Hamiltonian Monte Carlo (HMC) method for sampling from the posterior distribution (7). HMC simulates a Markov chain from the invariant distribution

$$P(\mathbf{p}, \mathbf{q}) = \frac{1}{Z} e^{-H(\mathbf{p}, \mathbf{q})}, \quad (9)$$

where \mathbf{p} are the parameters of interest (6), $\mathbf{q} \sim N(0, \mathbf{M})$ are auxiliary momentum variables which are conjugate and independent of \mathbf{p} , Z is a normalization constant, \mathbf{M} is a mass matrix and H is the Hamiltonian

$$H(\mathbf{p}, \mathbf{q}) = -\ell(\mathbf{p}) + \frac{1}{2} \mathbf{q}' \mathbf{M}^{-1} \mathbf{q}. \quad (10)$$

By marginalizing out the auxiliary momentum variables one obtains a sample from the posterior distribution of \mathbf{p} . For more details see D.

For HMC, the ability to effectively compute the gradient of (7) is vital. Using the chain rule we have

$$\begin{aligned} \frac{d\ell}{dp_i} &= \sum_{j=1}^n \frac{\partial \ell_{like}^j}{\partial C(t_0 + j)} \frac{\partial C(t_0 + j)}{\partial p_i} + \frac{\partial \ell_{like}}{\partial p_i} + \frac{\partial \ell_{prior}}{\partial p_i} \\ &= \sum_{j=1}^n \left(\frac{\partial \ell_{like}^j}{\partial C(t_0 + j)} \left(\frac{\partial C_I(t_0 + j)}{\partial p_i} - \frac{\partial C_I(t_0 + j - 1)}{\partial p_i} \right) + \frac{\partial \ell_{like}^j}{\partial p_i} \right) + \frac{\partial \ell_{prior}}{\partial p_i}. \end{aligned}$$

The term inside the inner parentheses is related with the notion of sensitivity, $\mathbf{s}_i(t)$, which broadly speaking measures the dependence of a compartment on the parameters of the model. More specifically,

$$\mathbf{s}_i(t) = \frac{\partial \mathbf{y}(t)}{\partial p_i} = (\partial_{p_i} y_1(t), \dots, \partial_{p_i} y_{M+K+3}(t))' = (s_{i,1}(t), \dots, s_{i,M+K+3}(t)),$$

and obeys the following equations

$$\dot{\mathbf{s}}_i(t) = \frac{d\mathbf{s}_i(t)}{dt} = \frac{\partial \mathbf{f}(t)}{\partial \mathbf{y}} \mathbf{s}_i(t) + \frac{\partial \mathbf{f}(t)}{\partial p_i}, \quad \text{with initial condition } \mathbf{s}_i(t_0), \quad (11)$$

which comes from the interchange property of partial and ordinary differentiation and the chain rule applied to (4). With a bit of algebra and using the notion of sensitivities one obtains

$$\frac{d\ell}{dp_i} = \begin{cases} \sum_{j=1}^n \frac{\partial \ell_{like}^j}{\partial C(t_0 + j)} (s_{i,M+K+3}(t_0 + j) - s_{i,M+K+3}(t_0 + j - 1)) \\ \quad + \frac{\partial \ell_{prior}}{\partial p_i} & i = 0, 1, 2, 5, \dots, m + 4 \\ \sum_{j=1}^n \frac{\partial \ell_{like}^j}{\partial p_i} + \frac{\partial \ell_{prior}}{\partial p_i} & i = 3 \\ \frac{\partial \ell_{prior}}{\partial p_i} & i = 4 \end{cases} \quad (12)$$

and

$$\begin{aligned} \frac{\partial \ell_{like}^j}{\partial C(t_0 + j)} &= \frac{\tilde{C}_{t_0+j}}{\eta(t_0+j)} - \frac{\tilde{C}_{t_0+j} + \phi}{C(t_0 + j) + \phi}, & \frac{\partial \ell_{like}^j}{\partial p_i} &= -\delta_{i3} \left(\psi \left(\frac{\tilde{C}_{t_0+j}}{\eta(t_0 + j)} + \phi \right) - \psi(\phi) \right. \\ & & & \left. + \frac{C(t_0 + j) - \frac{\tilde{C}_{t_0+j}}{\eta(t_0+j)}}{C(t_0 + j) + \phi} + \log(\phi) - \log(C(t_0 + j) + \phi) \right) \phi^2. \end{aligned}$$

Here $\psi(x) = \frac{d}{dx} \log(\Gamma(x)) = \frac{\Gamma'(x)}{\Gamma(x)}$ denotes the digamma function and δ_{ij} is the usual notation for the Kronecker delta, i.e., $\delta_{ij} = 1$ if $i = j$ and 0 otherwise. Once priors are chosen, computing $\frac{\partial \ell_{prior}}{\partial p_i}$ is also analytical.

We notice that both the log posterior ℓ (7) and its gradient $\frac{d\ell}{d\mathbf{p}}$ (12) are expressed analytically. This can remarkably facilitate sampling with HMC. In our setting, the only elements that are not analytically computable are the solutions of the ODE system (4) and its sensitivities. However, both can be obtained by solving numerically the extended ODE system

$$\begin{aligned} \dot{\mathbf{y}}(t) &= \mathbf{f}(t, \mathbf{y}, \mathbf{p}), & \mathbf{y}(t_0) &= (N - p_2, p_2, 0, \dots, 0, p_2)', \\ \dot{\mathbf{s}}_i(t) &= \frac{\partial \mathbf{f}(t)}{\partial \mathbf{y}} \mathbf{s}_i(t) + \frac{\partial \mathbf{f}(t)}{\partial \mathbf{p}_i}, & \mathbf{s}_i(t_0) &= (-\delta_{i2}, \delta_{i2}, 0, \dots, 0, \delta_{i2})'. \end{aligned} \quad (13)$$

Note that (13) is a system of $(M + K + 3) + (M + K + 3) \times (m + 3)$ ODEs, where $M + K + 3$ is the number of compartments, and $m + 3$ is the number of parameters involved in the ODEs. For implementation the size of the system can be slightly reduced, but for ease of notation we maintain it like this. We stress that $\mathbf{s}_3(t) = (0, \dots, 0)'$ and $\mathbf{s}_4(t) = (0, \dots, 0)'$ for any $t \geq 0$ since $p_3 = \phi^{-1}$ and $p_4 = \tau$ do not appear in the ODEs or the initial conditions and, hence, there is no need to incorporate the sensitivity for p_3 and p_4 in the system of ODEs. This results in only $m + 3$ parameters required to solve the ODEs which are solely related to the dynamic system. To solve (13), an ODE solver with forward sensitivity capabilities (see section 2.6 in [25]), such as, for example, CVODES in the C package SUNDIALS ([25]) is needed. We provide expressions for the Jacobian matrices $\frac{\partial \mathbf{f}(t)}{\partial \mathbf{y}}$ and $\frac{\partial \mathbf{f}(t)}{\partial \mathbf{p}}$ in B.

2.4 Implementation

The implementation of the proposed Hamiltonian-based sampling strategy is summarized in Algorithm 1. The overall procedure consists of three major steps: (1) Initialization, (2) Sampling and (3) Output. Input data include daily incidence data ($\{\tilde{C}_{t_0+j}\}_{j=1}^n$), initial values of model parameters (\mathbf{p}^0), a parameter associated with a gradient descent step (`learning_rate`), initial parameters for the Hamiltonian-based sampler (`HMC_parameters`), and the size of the Markov chain (N_{MC}). The following three steps precede Algorithm 1. First, one has to choose values for M and K in the $SE_M I_K R$ model. This is left to the user's discretion, who may be influenced by some external information, or may rely on trial and error. For example, if distributions for the infectious and the exposed period are empirically known, appropriate values of M and K can be chosen so that the corresponding Erlang distributions best fit the empirical ones. However, it is advisable to consider that an increase in M and K results in an increase in computation time.

The second step is the choice of m , the number of B-spline basis functions. Here, a simple strategy is to fix d , the degree of the spline polynomials (usually a good choice is $d = 3$), and then select the smallest value Q , the number of knots (which fixes $m = Q + d - 1$), for which a Bayesian

Algorithm 1 Hamiltonian-based Sampling Strategy

Input: $data = \{\tilde{C}_{t_0+j}\}_{j=1}^n, \mathbf{p}^0, \text{learning_rate}, \text{HMC_parameters}, N_{MC}$

```
1: Initialization
2:  $\mathbf{p}^0 \leftarrow$  Gradient descent with learning_rate starting at  $\mathbf{p}^0$ 
3:  $\mathbf{p}^0, \text{HMC\_parameters} \leftarrow$  tuning procedure based on  $\mathbf{p}^0$  and HMC_parameters
4:  $\mathbf{q}^0 \leftarrow$  draw from momentum distribution
5: Sampling
6: for  $1 \leq i \leq N_{MC}$  do
7:    $\mathbf{p}(0) \leftarrow \mathbf{p}^{i-1}$ 
8:    $\mathbf{q}(0) \leftarrow$  draw from momentum distribution (HMC) or use partially updated momentum based on  $\mathbf{q}^{i-1}$  (GHMC)
9:    $(\mathbf{p}^*, \mathbf{q}^*) \leftarrow$  evolve the system using Hamiltonian dynamics with Hamiltonian  $H$  and HMC_parameters for data
10:    $accep\_prob = \min\{1, e^{-(H(\mathbf{p}^*, \mathbf{q}^*) - H(\mathbf{p}(0), \mathbf{q}(0)))}\}$ 
11:   Metropolis test (accepts the proposal with the probability accep_prob):
12:    $u \sim U(0, 1)$ 
13:   if  $u < accep\_prob$  then
14:      $\mathbf{p}^i \leftarrow \mathbf{p}^*$  (Accept)
15:      $\mathbf{q}^i \leftarrow \mathbf{q}(0)$ 
16:   else
17:      $\mathbf{p}^i \leftarrow \mathbf{p}(0)$  (Reject)
18:      $\mathbf{q}^i \leftarrow -\mathbf{q}(0)$ 
19:   end if
20: end for
```

Output: A sample from the posterior distribution of model parameters \mathbf{p} (6).

P-spline regression can fit well enough all peaks and valleys of the daily incidence data. We opt to use the smallest value, since an increase in m enlarges the number of parameters to sample, which is the single most expensive computational step.

The third preceding step is the choice of a sensible enough initial value \mathbf{p}^0 of model parameters (6). This is important since nonsensical values may result in errors in the numerical integration of the ODE systems required in lines 2, 3 and 9 in Algorithm 1. We recommend to use some a priori values for such parameters as α, γ, E_0, I_0 and ϕ^{-1} , which can come from different origins: the literature available for similar diseases, expert knowledge, synthetic examples mimicking the data or sampling from the prior distributions. We also propose to use a constant transmission rate as initial guess, i.e. $\beta_1^0 = \dots = \beta_m^0 = \beta_{fixed}$, to obtain a classical $SE_M I_K R$ model as the initial point.

The selected \mathbf{p}^0 can be further refined by applying the gradient descent (ascent) (line 2 in Algorithm 1), which takes the parameters closer to the maximum of the log-posterior. The choice of the gradient descent optimization algorithm is natural for the proposed approach due to the ready available gradients. This improvement of the initial value helps a subsequent Markov chain to avoid errors in the integration step in lines 3 and 9 of Algorithm 1 and to compromise further development of the chain.

An additional effort may be needed to work out the close to optimal settings for exploring the posterior distribution. Precisely, line 3 is concerned with the tuning of the free parameters and settings required to run a Hamiltonian-based sampler in Algorithm 1. The complete specifications of a tuning strategy are beyond the scope of this work and will be explored in a related article. Here we just notice that the tuning procedure used in this study nominates an optimal numerical

integrator and returns the close to optimal values for an integration step size and Hamiltonian trajectory’s length.

Lines 6 to 19 in Algorithm 1 encode an HMC or a Generalized Hamiltonian (Hybrid) Monte Carlo (GHMC), depending on the user’s preference for the momentum update procedure. For some details on HMC/GHMC see D and for a more detailed overview we refer the reader to [44],[28] and [50].

The output of Algorithm 1 is a posterior sample of \mathbf{p} , i.e. a credible range of parameter values for the model (7) obtained by upgrading in a rigorous manner the prior knowledge using available data.

3 Data

In this section we present a brief overview of the synthetic data that we use to calibrate and explore the behaviour of the proposed methodology, and the real data to which we apply our approach.

3.1 Synthetic data

To obtain a meaningful synthetic dataset, we aim to emulate a plausible real situation. For this, we proceed as follows. The population size N is fixed to 2189138, i.e. the population of the Basque Country as given by the Spanish National Statistical Institute (INE in Spanish) for the year 2020 (available at the following link). The model parameters \mathbf{p}^{syn} are then refined by solving numerically (2) for a SEI_3R model at varying values of \mathbf{p}^{syn} until two waves, i.e., two peaks of daily incidence separated by a region of much lower incidence, in a period of 100 days, are obtained. We choose a SEI_3R model to go beyond a standard case where the ground truth is a SEIR model. Specifically, α, γ, E_0 and ϕ are fixed to reasonable values for a SARS virus (see (14)) and the parameters a, b of a transmission function

$$\beta(t; a, b) = \frac{e^{\sin(2\pi t/a) - t/a}}{b},$$

are varied until two waves are obtained (we consider $a = 50$ and $b = 4$). Then, a cubic P-spline approximation of the desired transmission $\beta(t; 50, 4)$ is used to fix m and β (see (1)).

The resulting parameters are:

$$\begin{aligned} \mathbf{p}^{syn} = & (\alpha = 0.5, \gamma = 0.1, E_0 = 10, \phi^{-1} = 0.1, \beta_1 = -1.8699, \beta_2 = -1.3014, \\ & \beta_3 = -0.2422, \beta_4 = -1.5110, \beta_5 = -3.3045, \beta_6 = -3.0917, \beta_7 = -1.5683, \\ & \beta_8 = -1.5705, \beta_9 = -3.4479, \beta_{10} = -4.5214, \beta_{11} = -3.3348, \beta_{12} = -2.8091). \end{aligned} \quad (14)$$

The numerical solution of (2) for a SEI_3R model with parameters \mathbf{p}^{syn} , $\{C^{syn}(j)\}_{j=1}^{100}$, is used to yield

$$\tilde{\mathbf{C}}^{syn} = \{\tilde{C}_j^{syn} : \text{draw from } \textit{NegativeBinomial}(C^{syn}(j), \phi^{-1} = 0.1)\}_{j=1}^{100}.$$

The dataset $\tilde{\mathbf{C}}^{syn}$ (black dots in Figure 2) is the one we use in our synthetic experiments.

3.2 COVID-19 daily incidence data

The COVID-19 daily incidence data used in this work was obtained from the Spanish National Epidemiological Center (CNE in Spanish). The data is available at the tab ‘Documentación y Datos’ in this link.

The data collection started on the 1st of January 2020 when the first positive case was detected in Madrid. As a starting point for the spread of the disease we consider the first day when a positive case is followed by at least one more positive case in the following 7 days. This gives different starting points for different autonomous communities, since the conditions we assume as the starting point of the transmission were fulfilled at different points in time. As we are interested in the Basque Country data, we take the 10th of February 2020 as an initial moment of the pandemic and the 31st of January 2021 as an ending point of the data series in order to avoid the effect of vaccination. Vaccination in Spain started in early January 2021, and was relatively slow at the beginning, hence until the end of January it was almost negligible for our purposes.

Results and discussion

The results of numerical experiments on the synthetic and real data, as well as the discussion of the behaviour of the developed methods, are provided in this section.

Case study 1: Synthetic data

Here we use the synthetic data introduced above in order to validate the proposed spline-based modelling approach and get a deeper insight into its behavior. Also, comparisons with a corresponding diffusion-based approach are presented. In particular, following [16] and with the help of the R-package `rbi` [27], we implemented SIR/SEIR-like dynamic models with a time-dependent transmission rate modelled by a diffusion process (i.e., given by Stochastic Ordinary Differential Equations, SODEs; see C for details). This provided us with a good baseline for investigating the behaviour of the proposed spline-based dynamic models $SE_M I_K R$ (2) and $SI_K R$ ((17) in A) combined with (5) against the diffusion-based $SE_M I_K R$ and $SI_K R$ (see, respectively, (21) and (22) in C) also combined with (5).

To use the Hamiltonian-based Monte Carlo described in Algorithm 1 along with the spline-based dynamic models introduced in this work we selected the following prior distributions:

$$\begin{aligned} \alpha_{HMC} &\sim N(0.5, 0.05^2), & \gamma_{HMC} &\sim U(0.095, 0.105), & E_{0,HMC} &\sim N(10, 1), \\ I_{0,HMC} &\sim N(10, 1), & \phi_{HMC}^{-1} &\sim Exp(10), & \tau_{HMC} &\sim InverseGamma(1, 0.005). \end{aligned} \quad (15)$$

In addition, a prior distribution for the coefficients, β , associated with the transmission rate was chosen as discussed in Bayesian set-up section (see equation (8)). Since we had access to the ground truth, we chose the number of cubic B-spline basis functions to be the true one, i.e., $m = 12$ in (1) (see (14)). Note that for γ_{HMC} we chose a prior distribution with compact support, centred around the true value and small variance. The reason for this choice can be justified as follows. Recall that the observed data correspond to daily incident case counts. As such, the data do not contain enough information regarding what is causing a large (small) number of new reported cases: either a large (small) transmission rate or a small (large) value for γ (the inverse of the recovery time). That is, different combinations of transmission rates and recovery times may give rise to similar observed incidence data (these model parameters are not identifiable). Due to the previous considerations and that our main interest is the transmission dynamics, it is sound to impose strong restrictions on γ and see if one can recover the generators transmission rate, $\beta(t)$. All in all, the proposed priors either codify confidence in values, as for α_{HMC} , γ_{HMC} , $E_{0,HMC}$ and $I_{0,HMC}$, force dispersion ϕ^{-1} to be close to 0, or provide almost no prior knowledge on the transmission rate β , except the smoothness conditions imposed by the B-spline basis and τ .

Following the strategy described in Algorithm 1, we started with $\mathbf{p}^0 = (\alpha^0, \gamma^0, E_0^0, \phi^{-1,0}, \beta_1^0 = \dots = \beta_{12}^0 = -1.6)$ (SEIR models) or $\mathbf{p}^0 = (\gamma^0, I_0^0, \phi^{-1,0}, \beta_1^0 = \dots = \beta_{12}^0 = -1.6)$ (SIR models) (in both cases, $\alpha^0, \gamma^0, E_0^0, I_0^0$ were draws from $\alpha_{HMC}, \gamma_{HMC}, E_{0,HMC}, I_{0,HMC}$ respectively, and $\phi^{-1,0}$ was fixed to 0.005 to stay close to the data) and performed 3000 gradient descent steps with `learning_rate` 10^{-6} for SIR and SEIR, and 10^{-7} for SI₃R and SEI₃R. This resulted in 4 different sets of starting parameters. To initialise the tuning step of Algorithm 1 (line 3) only a few initial sampling parameters are required as `HMC_parameters`. Here, a time step was set to 0.0001, which was small enough to avoid integration stability issues, an initial trajectory length for the integration method (symplectic method) was set to 1, and a mixing parameter for the momentum update was set to $\psi = 0.5$. For more details on these parameters we refer to D and references therein. The sampling parameters were then refined with the help of the in-house procedure (to be presented in a separate work) and used along with starting points for the model to run 10 chains of GHMC for 1000 burn-in and 10000 production steps. The number of production steps was chosen to get a Gelman-Rubin reduction factor (see [7]) close to 1 (from a visual inspection) for the majority of parameters.

Regarding the diffusion-based models, the parameter estimation for such models is performed using a sophisticated particle filter MCMC sampler, called SMC² ([11]). The prior distributions used in the case were

$$\begin{aligned} \alpha_{SMC^2} &\sim \alpha_{HMC}, & \gamma_{SMC^2} &\sim \gamma_{HMC}, & E_{0,SMC^2} &\sim E_{0,HMC}, & I_{0,SMC^2} &\sim I_{0,HMC} \\ \phi_{SMC^2}^{-1} &\sim U(0.01, 0.5), & \sigma_{SMC^2} &\sim U(0.01, 1), & \beta_{0,SMC^2} &\sim U(0.1, 1). \end{aligned} \quad (16)$$

Note that for α, γ, E_0 and I_0 we considered the same prior distributions as in the Hamiltonian-based Monte Carlo approach (see (15)). However, for ϕ^{-1} (the dispersion parameter in (5)) we chose a uniform prior. The reason for this choice (based on trial and error) comes from the complete failure of SMC² when initialised with the well grounded exponential prior used for the proposed spline-based dynamic models.

Before proceeding, we briefly describe how SMC² works. At $t = 0$ it samples N_p particles (values) from the prior distribution of the parameters (16), i.e., $\{\mathbf{p}^i = (\alpha_i, \gamma_i, E_{0,i}, \phi_i^{-1}, \sigma_i, \beta_{0,i})\}_{i=1}^{N_p}$ for SEIR models and $\{\mathbf{p}^i = (\gamma_i, I_{0,i}, \phi_i^{-1}, \sigma_i, \beta_{0,i})\}_{i=1}^{N_p}$ for SIR models. Also, for each \mathbf{p}^i , at each time step t it samples N_x instances of the stochastic $\beta(t)$ and evolves the trajectories of the mechanistic dynamics (the SODEs (21) and (22) in C), which are linked to the observations via (5). Next, the parameters are reweighted based on the conditional probability of the observed value at time t , $P(\tilde{C}_t | \tilde{C}_{t-1}, \dots, \tilde{C}_1, \mathbf{p}^i)$. If a degeneracy criteria is reached at time t (based on the weights of the proposed parameters) there is a rejuvenation mechanism that proposes, accepts or rejects new candidates. Therefore, SMC² returns a sample that is in correspondence with the evidence at each time t . This means that at time $t = 100$ (the last time point of the synthetic data) the posterior sample obtained by SMC² is comparable to the one obtained by the procedure described in Algorithm 1. 5 chains with 1000 production steps and 700 particles were run, where the number of production steps was chosen to get a Gelman-Rubin reduction factor close to 1.

The most important results are shown in Figures 2 and 3, more figures and details are provided in E.1.1.

Figure 2 depicts the posterior predictive checks on daily incidence for four different models – SIR, SI₃R, SEIR and SEI₃R – and their spline-based and diffusion-based versions, sampled with the GHMC and SMC² methodologies, respectively. As follows from the figure, the posterior predictive distribution samples for all models, regardless of the sampler, can generate data similar to the sample at hand (in black dots). Furthermore, the posterior predictive means, in solid lines, are very close to the true average of the generator (in dashed green). This means that our approach is

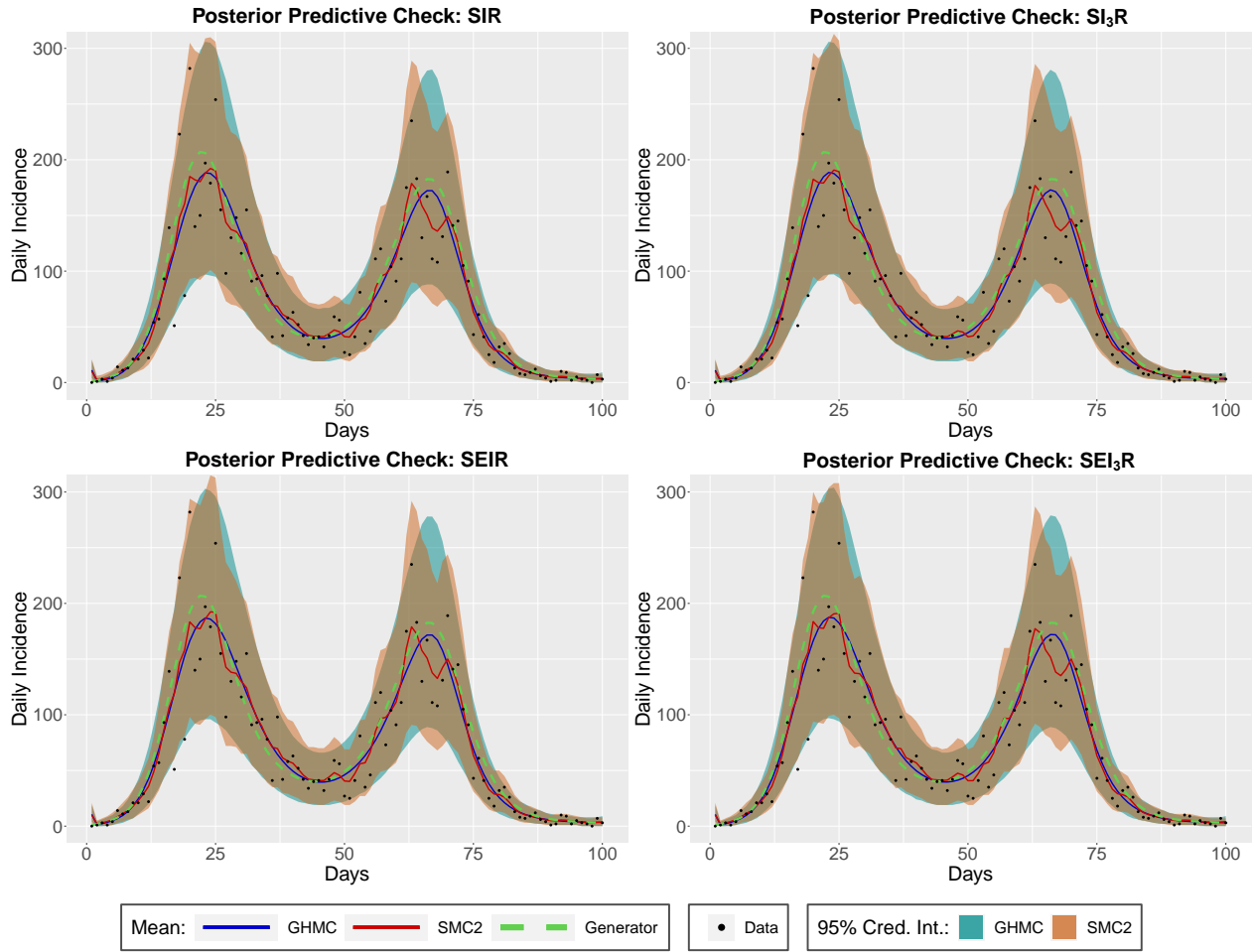


Figure 2: For the synthetic data: posterior predictive checks on daily incidence for a spline-based dynamics sampled with GHMC (combination of 10 chains with 10000 production steps) and a diffusion-based dynamics sampled with SMC² (combination of 5 chains with 700 particles and 1000 production steps) for four different compartmental models SIR, SI₃R, SEIR and SEI₃R. Dashed green lines represent the corresponding values of the true generator \mathbf{p}^{syn} (14).

comparable in its description of the data to the alternative diffusion-based mechanistic model (the SODEs (21) and (22) in C) with the sophisticated SMC² sampler.

In Figure 3, the estimated time-dependent transmission rates, $\beta(t)$, with the different models and samplers, are shown. Despite the clear similarities between SIR and SI₃R and also between SEIR and SEI₃R, significant differences between models with and without an exposed compartment are observed. For the models with an exposed compartment, SEIR and SEI₃R, the 95% credible intervals are close to containing or contain, respectively, the true values (in dashed green), while this is not the case for the models without an exposed compartment. It is worth noticing that the posterior median of $\beta(t)$, in solid lines, captures well the wave-like behaviour of the true generator. We see that the GHMC explores the space away from the initial transmission rate (in dashed purple) and produces results comparable to those of the SMC² procedure. Comparison of the posterior distributions of the epidemiologically relevant parameters can be found in Figures 8 - 11 in E.1.1. Notice that the best median $\beta(t)$ is obtained when we use the true model SEI₃R. The same conclusions can be seen for the time-dependent basic reproduction number, $R_0(t) = \beta(t)/\gamma$,

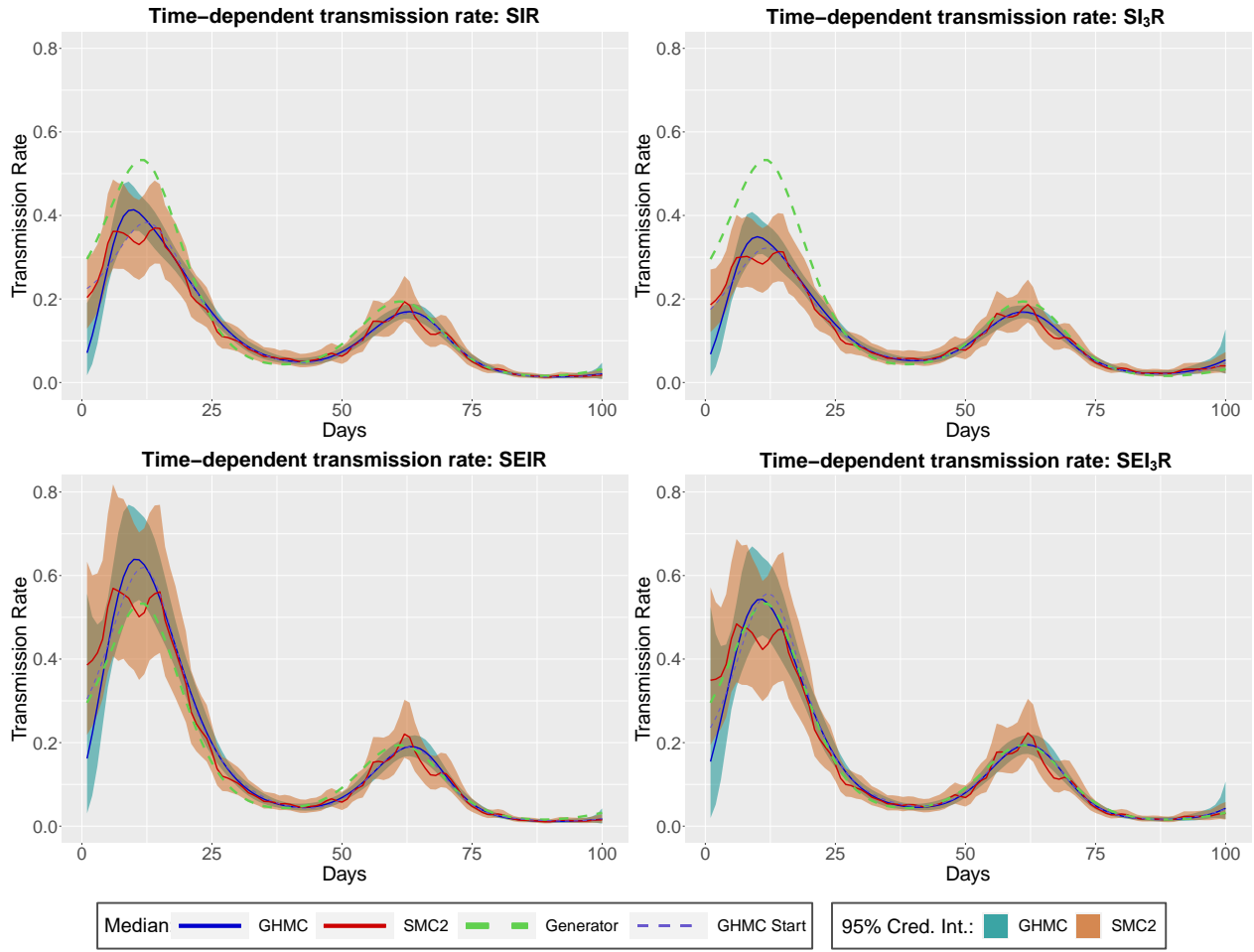


Figure 3: For the synthetic data: posterior medians (solid lines) and 95% credible intervals (shaded areas) of the time-dependent transmission rate, $\beta(t)$, for a spline-based dynamics sampled with GHMC (combination of 10 chains with 10000 production steps) and a diffusion-based dynamics sampled with SMC² (combination of 5 chains with 700 particles and 1000 production steps) for four different compartmental models SIR, SI_3R , SEIR and SEI_3R . Dashed purple lines represent the starting values of the GHMC chains corresponding to the result of the tuning step in Algorithm 1. Dashed green shows the corresponding values of the true generator \mathbf{p}^{syn} (14).

depicted in Web Figure 7 in E.1.1. This highlights the importance of the choice of model for recovering unobserved quantities such as the transmission rate and the basic reproduction number.

Noticeable differences between the two approaches are the following. The trajectories obtained with GHMC are smoother as a result of the choice in the mechanistic model of the transmission rate (1) which belongs to a space spanned by a B-spline basis. This regularity is not required when $\beta(t)$ is governed by a diffusion process. Additionally, in comparison with SMC², a Hamiltonian-based MC method allows for more flexibility with the choice of prior distributions, hence, for a more robust approach. For example, trail and error was needed to specify the prior on ϕ^{-1} (the dispersion parameter in (5)) for SMC², while Hamiltonian-based MC withstood much better the exponential prior. This is mainly due to the fact that the latter has access to the gradients of the log-likelihood and can soften the influence of the prior. It is worth mentioning that there is a significant difference on the priors on $\beta(t)$ for both procedures, which is due to the different mechanistic dynamics.

Finally, though both approaches are well suited to accommodate a flexible time-dependent transmission rate $\beta(t)$, the spline-based dynamic models have good differentiability properties, and therefore they are well adapted to any Hamiltonian-based MC methods. The diffusion-based models are not amenable to differentiation and hence advanced Sequential MC methods such as SMC² are required.

We remark that four different model families, with transmission rates modelled in different ways, and sampled with different techniques, can generate almost identical data (see Figure 2). This is a consequence of the fact that not only some parameters but also the model structure are not easily identifiable from incidence data [52]. This should be kept in mind when drawing conclusions from a model and when selecting prior distributions. Due to the great flexibility of the models there is a vast region of parameters (some without any epidemiological interest) which are able to represent the incidence data. This makes the problem of thoroughly sampling the posterior distribution quite hard. An example of these difficulties can be seen when we allow for a less restrictive prior on γ . Details and figures can be seen in E.1.2. There we see that very different combinations of γ and $\beta(t)$ can accurately describe the data at hand. Our advice is, when possible, to make use of epidemiological or other knowledge to introduce restrictive priors, since this can help to reduce the viable parameter regions.

Despite these difficulties, the proposed models and methodology were enough to retrieve plausible generators for the data and to capture the wave-like behaviour of the transmission-rate and the basic reproduction number, which are not directly observed. Therefore, with the proposed methods one can recover meaningful information about the transmission evolution of a disease. Our synthetic experiments show that, not surprisingly, the choice of models and samplers has an influence in the obtained transmission evolution, and practitioners should be aware of that.

Case study 2: Basque Country data

Next, the methods proposed in this work are applied to daily incidence data for the Basque Country. A crucial task is to provide adequate prior distributions for the parameters of interest. The synthetic example of the previous section supports choosing a strong prior on γ , while still leaving a lot of freedom to the time-dependent transmission rate $\beta(t)$ (for more details see Bayesian set-up section and equation (8) therein). Here we account for the fact that the study deals with a coronavirus and, therefore, there is a considerable prior knowledge about a plausible average recovery time. In particular, we consider $\gamma \in [1/30, 1]$. Another non-trivial choice is the prior on the initial infected population. For this, we just select a very low rate of initial infected population, i.e., around 1 infected for every 100000 individuals, which is a sensible choice for the very beginning of the spread of COVID-19 in the Basque Country. Hence, our choice for priors is the following

$$\begin{aligned} \alpha_{HMC} &\sim N(0.5, 0.05^2), & \gamma_{HMC} &\sim N_{[1/30,1]}(0.1, 0.015^2), & E_{0,HMC} &\sim N(21.88, 7.29^2), \\ I_{0,HMC} &\sim N(21.88, 7.29^2), & \phi_{HMC}^{-1} &\sim Exp(10), & \tau_{HMC} &\sim InverseGamma(1, 0.005). \end{aligned}$$

Where $N_{[a,b]}$ denotes a truncated normal distribution, which takes values on the interval $[a, b]$. The next step is to choose a proper value for $m = Q + d - 1$, the number of B-spline basis functions. A standard choice for the degree of the polynomials is $d = 3$ (i.e., cubic). In order to select an adequate number of internal knots Q , we applied Bayesian P-spline regression to the Basque Country Incidence data for $Q \in \{10, 11, \dots, 19, 20\}$ (Figure 4). The subjective strategy to choose the smallest Q -value that returns a fairly good regression of the incidence data results in $Q = 12$. This step is relatively inexpensive in terms of computational power.

For the choice of \mathbf{p}^0 we follow the same principle as in the synthetic example. $\alpha^0, \gamma^0, E^0, I^0$ were generated from the prior distributions. $\phi^{-1,0} = 0.005$ was fixed to favour the model being close to

P-spline regression

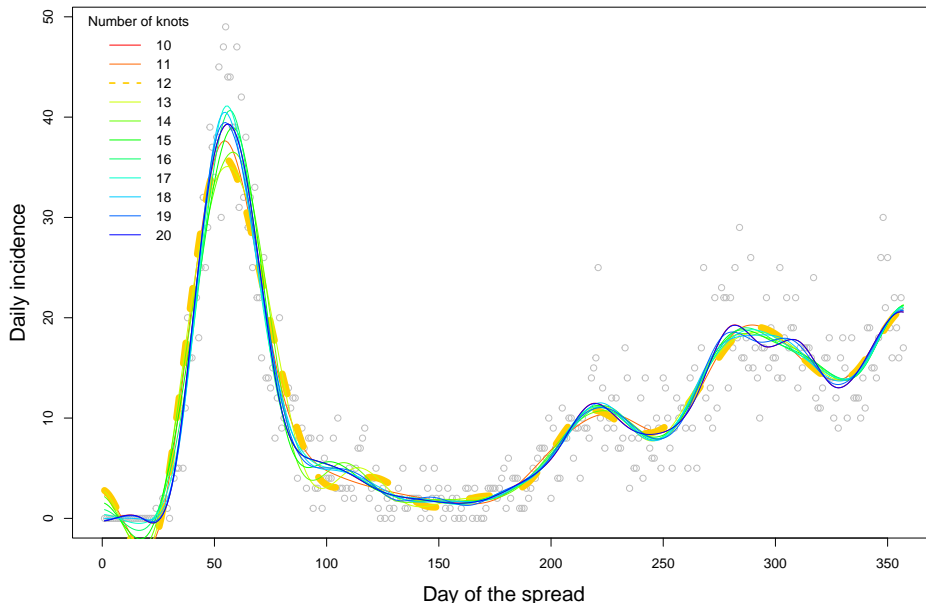


Figure 4: For the Basque Country data: estimated P-spline regression (posterior mean) on daily incidence data (grey dots) uncorrected for under-reporting for a different number of internal knots $Q = 10, \dots, 20$. The priors were chosen following the suggestions in [35]. 5000 MCMC production steps with a 1000 burn-in were taken.

the data. We set the initial spline coefficients to $\beta_1^0 = \dots = \beta_{15}^0 = -1.6$. 3000 gradient descent steps were performed with `learning_rate` = 10^{-7} for all models to obtain a more suitable \mathbf{p}^0 . Initial `HMC_parameters` were set to the same values as for the synthetic data, and further refined using the in-house procedure. We run 10 chains of GHMC for 1000 burn-in and 10000 production steps.

The main results of the proposed methods applied to the Basque Country data with corrections for under-reporting are shown in Figures 5 and 6. Additional results are provided in E, where the time dependent transmission rate is given in Web Figure 21, while the posterior densities of the relevant epidemiological parameters are depicted in Web Figures 22 and 23. To exemplify the behaviour of different models we choose, as in the synthetic example, four different compartmental models: SIR, SI_3R , SEIR and SEI_3R . The correction for under-reporting $\eta(t)$ in (5) is the following: $\eta(t) = 0.15$ for $0 < t \leq 92$, $\eta(t) = 0.15 + (0.54 - 0.15)(t - 92)/(231 - 92)$ for $92 < t < 281$, $\eta(t) = 0.54$ for $281 \leq t$. The under-reporting correction is a linear interpolation of the seroprevalence found in [41, 48], which reflects that at the beginning of May (day 92) only 15% and at mid November (day 281) only 54% of positive cases were reported in the Basque Country. The data corrected for under-reporting are depicted as black points and the original data as orange ones in Figure 5.

The posterior predictive check for all four models is shown in Figure 5. Clearly, all models are able to generate data similar to the observed one. We see that all models are essentially returning the same posterior predictive means and 95% predictive intervals. Hence, they are all plausible for describing a transmission of the disease when only daily incidence data are considered. Since we are interested in the effects of non-pharmacological measures taken by the state and local governments, we also graphically represent some of the most important ones, such as lockdowns and emergency protocols (in dot-dashed red), as well as the lifting and easing of these extreme measures (in dot-

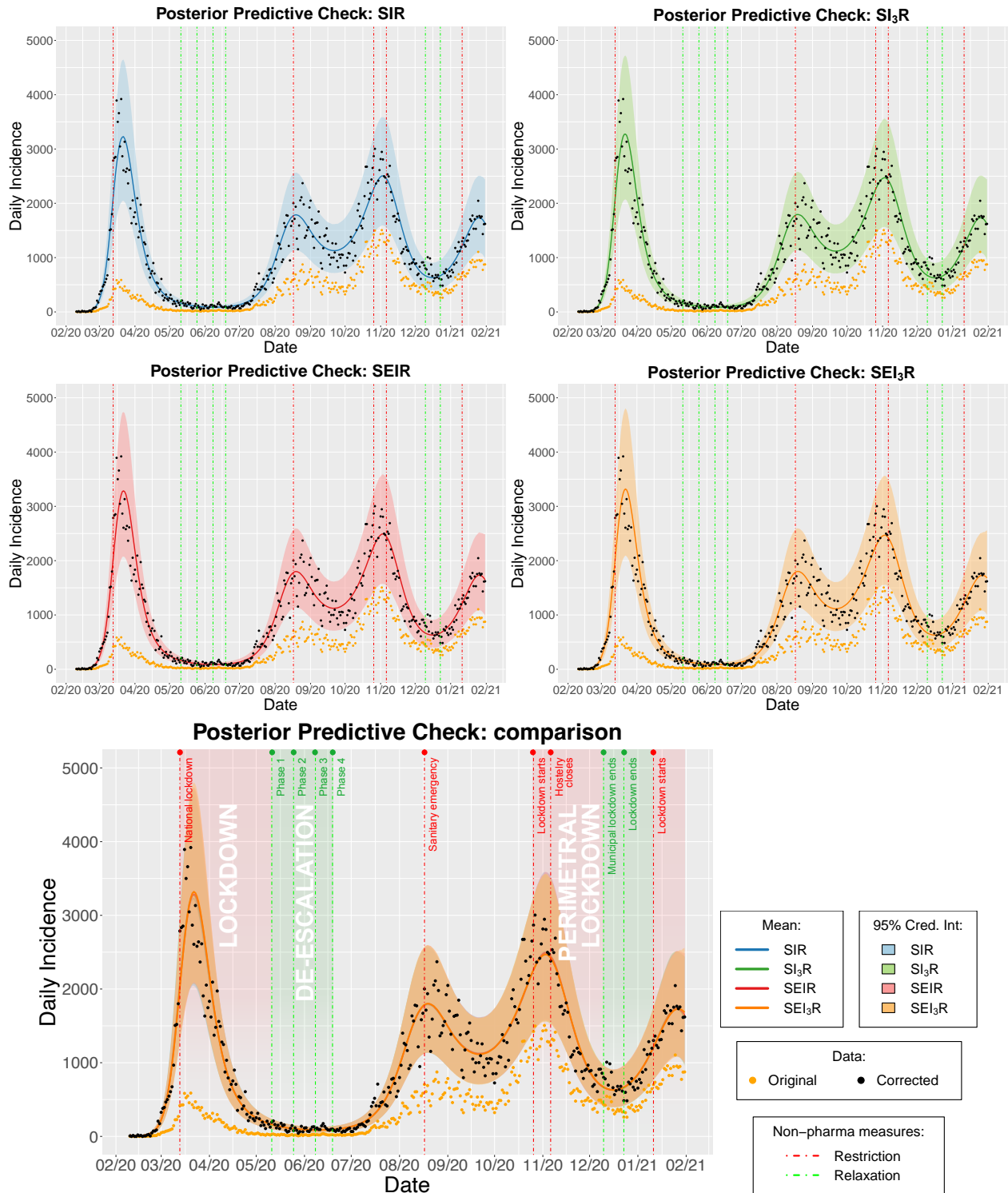


Figure 5: For the Basque Country data: posterior predictive checks on daily incidence data, corrected for under-reporting for the Basque Country, based on GHMC posterior samples for the model parameters of spline-based dynamic models (2) (or (17)) and (5). Results are shown for a combination of 10 chains with 10000 production steps. Four different compartmental models SIR, SI₃R, SEIR and SEI₃R are displayed.

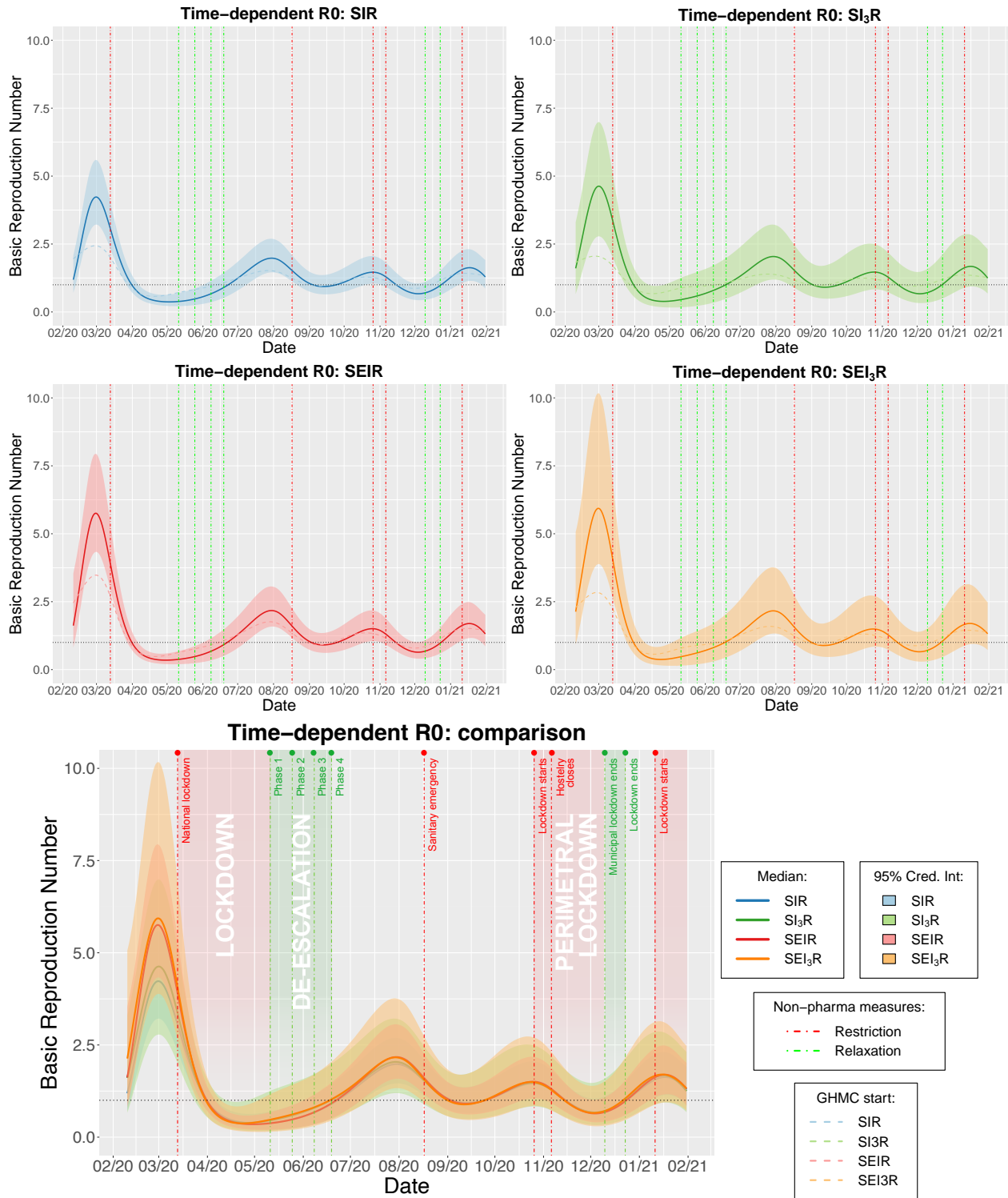


Figure 6: For the Basque Country data: posterior medians (solid lines) and 95% credible intervals (shaded areas) of the time-dependent basic reproduction number, $R_0(t) = \beta(t)/\gamma$, for spline-based dynamic models (2) (or (17)) and (5) sampled with GHMC. Results are shown for a combination of 10 chains with 10000 production steps. Four different compartmental models SIR, SI_3R , SEIR and SEI_3R are displayed. Dashed grey lines represent the starting values of the chains corresponding to the tuning step in Algorithm 1.

dashed green). In the incidence data plots, almost all extreme restrictive measures are taken before the peaks of daily cases. Similarly, all easing measures seem to be followed by an increase in daily incidence.

A relevant question to pose is how these non-pharmacological measures correlate with the transmission dynamics of the disease. In the time-dependent setting proposed in this work this information can be extracted from the observed changes in the basic reproduction number. Precisely, this can be seen in Figure 6, where the posterior median and 95% credible intervals for the basic reproduction number (R_0) for all models are plotted, alongside the different measures taken in the Basque Country.

Recall that R_0 is a good indicator of the state of the disease transmission, with values below 1 indicating the dying out of the transmission and values above 1 implying the further propagation. The higher the value of R_0 the more individuals are infected on average by a single infectious individual. What we see in Figure 6 is that all models agree that there were only two time intervals where median R_0 went consistently below 1 (a dotted grey line). One was during the state wise lockdown that started in the middle of March 2020 and the other one during the lockdown of the Basque Country commenced at the end of October 2020. We also see that all models indicate that during restrictive measures there is a decrease in transmission, whereas the ease of restriction comes together with an increase in transmission. Additionally, there is agreement between the models that the highest transmission occurred in the first wave, and the consequent waves had lower transmission rates, though high enough to keep the pandemic going on. A final observation to make is that the restrictions in the third and fourth waves seem to precede or coincide with the peak of the transmission rate, while the restrictive measures in the first two waves were likely taken after the peaks in transmission. We think that one should be extremely cautious when trying to interpret this last observation as a measure of the efficacy of non-pharmacological actions, and we abstain from doing so.

4 Conclusions

In this work, we have adapted popular and efficient families of compartmental models, such as the SI_{KR} and $SE_M I_{KR}$ models to a time-dependent transmission rate represented using a B-spline basis expansion to capture a wide range of transmission patterns. Based on these models, we introduced a generative mechanism suitable for the particularities of COVID-19. A Hamiltonian-based Monte Carlo procedure to obtain posterior samples of the model parameters was introduced in accordance with the paradigm of dynamic models. Hence, methods that capture both uncertainty in the data and in the model parameters were provided. All presented methods have been implemented in a user-friendly tool, based on `C` and `R` [49], and can be made available under petition (we are working on making it freely available online). The synthetic case study and the comparison with an advanced alternative method shows that our procedure is competitive and allows us to obtain meaningful information about the relative variation in time of the transmission process, which we recall, is not observed and hence is not used in the posterior log-likelihood.

Experiments on the COVID-19 daily incidence data for the Basque Country show that the presented methods are able to capture the variability of the transmission process of the disease causing a devastating pandemic. We want to remark that we are not promoting a single best model that captures the information in a dataset. On the contrary we are offering a broad family of models that can be used for that purpose. The decision of which concrete model to use is left to the expertise of a user. However, based on our experiments, we strongly suggest practitioners use in parallel a variety of models and prior distributions in order to obtain robust conclusions. Additionally, our

methods' execution times (including tuning and sampling, in the worst cases always lower than 24 hours for the Basque Countr data) allow us to monitor daily, or every two days, the evolution of the transmission of the disease. We are working on improving computational efficiency to reduce the execution times of our methods.

Furthermore, the proposed methods are generalizable to situations that have not been discussed in this work. To begin with, it is conceptually straightforward, although technically involved, to produce predictions for the future transmission of a disease of interest. Models more suitable for a particular modelling purpose can easily replace the Negative Binomial model presented in (5). Another possible generalisation is to use SEIR-like models with mortality and hospitalisation where the time-dependent mortality and hospitalisation rates are modelled using B-splines. In that situation, computing the semi-analytical form of the gradients may be more involved, but it is completely feasible. A last notable extension is that we can compute the Hessian of the log-posterior (see (20) in B) in a similar fashion as the gradient, due to the good differentiability properties of the considered models, which is useful for some extensions of HMC and applications of the models in other Machine Learning procedures [50].

Acknowledgments

This research was partially supported by projects PID2019-104927GB-C22 (AEI; LN, EA), MTM2017-86061-C2-1-P (AEI/FEDER, UE; HIV), by the Ramón y Cajal Grant RYC2019-027534-I (MXRA), by grant LCF/BQ/DI20/11780022 (LN), by the Basque Government through the BERC 2018-2021 program (All) and Elkartek projects KK-2021/00022 (LN, EA), KK-2021/00064 (LN, EA) and KK-2022/00006 (EA), by the Spanish Ministry of Science and Innovation and AEI (BCAM Severo Ochoa accreditation CEX2021-001142-S; All), and by grants VA005P17 and VA002G18 (Junta de Castilla y León; HIV). We want to thank Delia Mozo for her help with the design of some of the figures. We also are grateful to Moumita Das for helpful comments and discussions.

References

- [1] M. Aguiar, E. Millán Ortuondo, J. Bidaurrezaga Van-Dierdonck, J. Mar, and N. Stollenwerk. Modelling COVID 19 in the Basque Country from introduction to control measure response. *Scientific Reports*, 2020.
- [2] D. Anderson and R. Watson. On the spread of a disease with gamma distributed latent and infectious periods. *Biometrika*, 67:191–198, 1980.
- [3] J. Arino and S. Portet. A simple model for COVID-19. *Infectious Disease Modelling*, 5:309–315, 2020.
- [4] M. Baguelin, G. F. Medley, E. S. Nightingale, K. M. O'Reilly, E. M. Rees, N. R. Waterlow, and M. Wagner. Tooling-up for infectious disease transmission modelling. *Epidemics*, 32, 2020.
- [5] N. T. J. Bailey. Some stochastic models for small epidemics in large populations. *Journal of the Royal Statistical Society. Series C*, 13(1):9–19, 1964.
- [6] A. L. Bertozzia, E. Franco, G. Mohler, M. B. Short, and D. Sledge. The challenges of modeling and forecasting the spread of COVID-19. *PNAS*, 117:16732–16738, 2020.

- [7] Stephen P Brooks and Andrew Gelman. General methods for monitoring convergence of iterative simulations. *Journal of computational and graphical statistics*, 7(4):434–455, 1998.
- [8] T. Carletti, D. Fanelli, and F. Piazza. COVID-19: The unreasonable effectiveness of simple models. *Chaos, Solitons & Fractals: X*, 5, 2020.
- [9] C. Carroll, S. Bhattacharjee, Y. Chen, P. Dubey, J. Fan, Á. Gajardo, X. Zhou, H.-G. Müller, and J.-L. Wang. Time dynamics of COVID-19. *Scientific Reports*, 2020.
- [10] A. Chatzilena, E. van Leeuwen, O. Ratmann, M. Baguelin, and N. Demiris. Contemporary statistical inference for infectious disease models using Stan. *Epidemics*, 29, 2019.
- [11] N. Chopin, P. E. Jacob, and O. Papaspiliopoulos. SMC² : an efficient algorithm for sequential analysis of state space models. *Journal of the Royal Statistical Society. Series B*, 75(3):397–426, 2013.
- [12] J.-P. Chretien, D. George, J. Shaman, R. A. Chitale, and F. E. McKenzie. Influenza forecasting in human populations: A scoping review. *PLOS ONE*, 9(4), 2014.
- [13] F. C. Coelho, C. T. Codec, and M. G. M. Gomes. A Bayesian framework for parameter estimation in dynamical models. *PLoS ONE*, 6(5), 2011.
- [14] A. Cori, N. M. Ferguson, C. Fraser, and S. Cauchemez. A new framework and software to estimate time-varying reproduction numbers during epidemics. *American Journal of Epidemiology*, 178(9):1505–1512, 2013.
- [15] P. Dierckx, editor. *Curve and Surface Fitting with Splines*. Oxford University Press, 1993.
- [16] J. Dureau, K. Kalogeropoulos, and M. Baguelin. Capturing the time-varying drivers of an epidemic using stochastic dynamical systems. *Biostatistics*, 14(3):541–555, 2013.
- [17] D. Faranda, I. Pérez Castillo, O. Hulme, A. Jezequel, J. S. W. Lamb, Y. Sato, and E. L. Thompson. Asymptotic estimates of SARS-CoV-2 infection counts and their sensitivity to stochastic perturbation. *Chaos*, 30, 2020.
- [18] N. M. Ferguson, D. Laydon, and G. Nedjati-Gilani et al. *Impact of non-pharmaceutical interventions (NPIs) to reduce COVID-19 mortality and healthcare demand*, volume Report 9. Imperial College London, 2020.
- [19] S. Flaxman, S. Mishra, A. Gandy, H. J. T. Unwin, T. A. Mellan, H. Coupland, C. Whitaker, H. Zhu, T. Berah, J. W. Eaton, M. Monod, A. C. Ghani, C. A. Donnelly, S. Riley, M. A. C. Vollmer, N. M. Ferguson, L. C. Okell, and S. Bhatt. Estimating the effects of non-pharmaceutical interventions on COVID-19 in Europe. *Nature*, 584, 2020.
- [20] G. Frasso and P. Lambert. Bayesian inference in an extended SEIR model with nonparametric disease transmission rate: an application to the Ebola epidemic in Sierra Leone. *Biostatistics*, 17(4):779–792, 2016.
- [21] S. Funk, A. Camacho, A. J. Kucharski, R. M. Eggo, and W. J. Edmunds. Real-time forecasting of infectious disease dynamics with a stochastic semi-mechanistic model. *Epidemics*, 22:56–61, 2018.

- [22] P. Girardi and C. Gaetan. An SEIR model with time-varying coefficients for analyzing the SARS-CoV-2 epidemic. *Risk Analysis*, 2021.
- [23] A. Hauser, M. J. Counotte, C. C. Margossian, G. Konstantinoudis, N. Low, C. L. Althaus, and J. Riou. Estimation of SARS-CoV-2 mortality during the early stages of an epidemic: A modeling study in Hubei, China, and six regions in Europe. *PLOS Medicine*, 17(7):e1003189, 2020.
- [24] H. Heesterbeek, R. M. Anderson, V. Andreasen, S. Bansal, D. De Angelis, C. Dye, K. T. D. Eames, W. John Edmunds, S. D. W. Frost, S. Funk, T. Deirdre Hollingsworth, T. House, V. Isham, P. Klepac, J. Lessler, J. O. Lloyd-Smith, C. J. E. Metcalf, D. Mollison, L. Pellis, J. R. C. Pulliam, M. G. Roberts, and C. Viboud. Modeling infectious disease dynamics in the complex landscape of global health. *Science*, 447:1–10, 2015.
- [25] A. C. Hindmarsh and R. Serban. *User Documentation for cvodes v5.3.0 (sundials v5.3.0)*. Center for Applied Scientific Computing Lawrence Livermore National Laboratory, USA, 2020.
- [26] H. G. Hong and Y. Li. Estimation of time-varying reproduction numbers underlying epidemiological processes: A new statistical tool for the COVID-19 pandemic. *PLOS ONE*, 15(7), 2020.
- [27] Pierre E. Jacob and Sebastian Funk. *rbi: Interface to 'LibBi'*, 2021. R package version 0.10.4.
- [28] A. D. Kennedy and B. Pendleton. Cost of the generalised hybrid Monte Carlo algorithm for free field theory. *Nuclear Physics B*, 607:456–510, 2001.
- [29] W. O. Kermack and A. G. McKendrick. A contribution to the mathematical theory of epidemics. *Proc. R. Soc. Lond. A*, 115:700–721, 1927.
- [30] S. Khailaie, T. Mitra, A. Bandyopadhyay, M. Schips, P. Mascheroni, P. Vanella, B. Lange, S. C. Binder, and M. Meyer-Hermann. Development of the reproduction number from coronavirus SARS-CoV-2 case data in Germany and implications for political measures. *BMC Medicine*, 2021.
- [31] T. Kneib. *Mixed model based inference in structured additive regression*. Ludwig–Maximilians–Universität München, 2005.
- [32] S. Koyama, T. Horie, and S. Shinomoto. Estimating the time-varying reproduction number of COVID-19 with a state-space method. *PLOS Computational Biology*, 2021.
- [33] O. Krylova and D. J. D. Earn. Effects of the infectious period distribution on predicted transitions in childhood disease dynamics. *Journal of the Royal Society Interface*, 10, 2013.
- [34] A. J. Kucharski, T. W. Russell, C. Diamond, Y. Liu, J. Edmunds, S. Funk, and R. M. Eggo. Early dynamics of transmission and control of COVID-19: a mathematical modelling study. *Lancet Infect Dis*, 20:536–558, 2020.
- [35] S. Lang and A. Brezger. Bayesian P-Splines. *Journal of Computational and Graphical Statistics*, 13 (1):183–212, 2004.

- [36] A. Leitao and C. Vázquez. The stochastic θ -SEIHRD model: Adding randomness to the COVID-19 spread. *Communications in Nonlinear Science and Numerical Simulation*, 115:106731, 2022.
- [37] M. Y. Li. *An Introduction to Mathematical Modeling of Infectious Diseases*. Springer, 2018.
- [38] Z. Liu, P. Magal, O. Seydi, and G. Webb. A COVID-19 epidemic model with latency period. *Infectious Disease Modelling*, 5:323–337, 2020.
- [39] A. L. Lloyd. Realistic distributions of infectious periods in epidemic models: Changing patterns of persistence and dynamics. *Theoretical Population Biology*, 60:59–71, 2001.
- [40] T.T. Marinov and R. S. Marinova. Dynamics of COVID-19 using inverse problem for coefficient identification in SIR epidemic models. *Chaos, Solitons & Fractals: X*, 2020.
- [41] Ministerios de Ciencia e Innovación y de Sanidad, Madrid. *Estudio ENE-COVID: Cuarta ronda estudio nacional de sero-epidemiología de la infección por SARS-COV-2 en España*, 2020.
- [42] M. Mofijur, I. M. R. Fattah, A. Alam, A. B. M. S. Islam, H. C. Ong, S. M. A. Rahman, G. Najafie, S. F. Ahmed, A. Uddin, and T. M. I. Mahlia. Impact of COVID-19 on the social, economic, environmental and energy domains: Lessons learnt from a global pandemic. *Sustainable Production and Consumption*, 26:343–359, 2021.
- [43] L. M. Murray. Bayesian state-space modelling on high-performance hardware using LibBi. *Journal of Statistical Software*, 67 (10), 2015.
- [44] R. F. Neal. MCMC using Hamiltonian dynamics. In S. Brooks, A. Gelman, G. Jones, and X.-L. Meng, editors, *Handbook of Markov Chain Monte Carlo*, chapter 5, pages 136–162. Chapman and Hall/CRC, 2011.
- [45] E. O. Nsoesie, J. S. Brownstein, N. Ramakrishnan, and M. V. Marathe. A systematic review of studies on forecasting the dynamics of influenza outbreaks. *Influenza and other respiratory viruses*, 8(3):309–316, 2014.
- [46] D. Osthus, J. Gattiker, R. Priedhorsky, and S. Y. Del Valle. Dynamic Bayesian influenza forecasting in the United States with hierarchical discrepancy (with discussion). *Bayesian Analysis*, 14(1):261–312, 2019.
- [47] G. Pillonetto, M. Bisiacco, G. Palù, and C. Cobelli. Tracking the time course of reproduction number and lockdown’s effect on human behaviour during SARS-CoV-2 epidemic: nonparametric estimation. *Scientific Reports*, 11, 2021.
- [48] M. Pollán, B. Pérez-Gómez, R. Pastor-Barriuso, J. Oteo, M. A. Hernán, M. Pérez-Olmeda, J. L. Sanmartín, A. Fernández-García, I. Cruz, N. Fernández de Larrea, M. Molina, F. Rodríguez-Cabrera, M. Martín, P. Merino-Amador, J. León Paniagua, J. F. Muñoz-Montalvo, F. Blanco, and R. Yotti. Prevalence of SARS-CoV-2 in Spain (ENE-COVID): a nationwide, population-based seroepidemiological study. *The Lancet*, 396(10250):535–544, 2020.
- [49] R Core Team. *R: A Language and Environment for Statistical Computing*. R Foundation for Statistical Computing, Vienna, Austria, 2023.

- [50] T. Radivojevic and E. Akhmatskaya. Modified Hamiltonian Monte Carlo for Bayesian inference. *Statistics and Computing*, 30:377–404, 2020.
- [51] A. Smirnova, L. deCamp, and G. Chowell. Forecasting epidemics through nonparametric estimation of time-dependent transmission rates using the SEIR model. *Bulletin of Mathematical Biology*, 81:4343–4365, 2019.
- [52] C. Souto-Maior. Multiple-serotype models of dengue virus transmission: simulation study and perspectives for the application of inference in epidemiological surveillance. *bioRxiv*, 2019.
- [53] T. Stocks, M. Höhle, and T. Britton. Model selection and parameter estimation for dynamic epidemic models via iterated filtering: application to rotavirus in Germany. *Biostatistics*, 21:400–416, 2020.
- [54] Q. Wang, S. Xie, Y. Wang, and D. Zeng. Survival-convolution models for predicting COVID-19 cases and assessing effects of mitigation strategies. *Frontiers in public health*, page 325, 2020.
- [55] X. Xu, T. Kypraios, and P. D. O’Neill. Bayesian non-parametric inference for stochastic epidemic models using Gaussian processes. *Biostatistics*, 17(4):619–633, 2016.
- [56] T. Yue, Z. Fan, B. Fan, Z. Du, J. P. Wilson, X. Yin, N. Zhao, Y. Wang, and C. Zhou. A new approach to modeling the fade-out threshold of coronavirus disease. *Science Bulletin*, 65, 2020.
- [57] J. Zelner, J. Riou, R. Etzioni, and A. Gelman. Accounting for uncertainty during a pandemic. *Patterns (New York, N.Y.)*, 2(8):100310, 2021.
- [58] J. Zhu and B. Gallego. Evolution of disease transmission during the COVID-19 pandemic: patterns and determinants. *Scientific Reports*, 11, 2021.

Appendix A SI_KR model

The dynamics for the SI_KR model can be described by the following system of ODEs:

$$\begin{aligned}
\frac{dS(t)}{dt} &= -\exp\left(\sum_{i=1}^m \beta_i B_i(t)\right) S(t) \frac{\sum_{j=1}^K I_j(t)}{N} = -\beta(t) S(t) \frac{I(t)}{N}, \\
\frac{dI_1(t)}{dt} &= \exp\left(\sum_{i=1}^m \beta_i B_i(t)\right) S(t) \frac{I(t)}{N} - K\gamma I_1(t), \\
\frac{dI_2(t)}{dt} &= K\gamma I_1(t) - K\gamma I_2(t), \\
&\dots, \\
\frac{dI_K(t)}{dt} &= K\gamma I_{K-1}(t) - K\gamma I_K(t), \\
\frac{dR(t)}{dt} &= \frac{d}{dt} (N - S(t) - I(t)) = K\gamma I_K(t), \\
\frac{dC_I(t)}{dt} &= \exp\left(\sum_{i=1}^m \beta_i B_i(t)\right) S(t) \frac{I(t)}{N},
\end{aligned} \tag{17}$$

with initial conditions:

$$S(t_0) = N - I_0, I(t_0) = I_1(t_0) = I_0, R(t_0) = 0, C_I(t_0) = I_0.$$

Using the parametrization

$$\begin{aligned}
\mathbf{y}(t) &= (y_1(t), y_2(t), \dots, y_{K+1}(t), y_{K+2}(t), y_{K+3}(t))' \\
&= (S(t), I_1(t), \dots, I_K(t), R(t), C_I(t))',
\end{aligned}$$

we obtain the following condensed form of the equations

$$\dot{\mathbf{y}}(t) = \frac{d\mathbf{y}(t)}{dt} = \mathbf{f}(t, \mathbf{y}, \mathbf{p}), \quad \mathbf{y}(t_0) = (N - I_0, I_0, 0, \dots, 0, I_0)'. \tag{18}$$

By combining equations (17) and the probabilistic model (5) in the main text, the parameters to estimate can be expressed as

$$\mathbf{p} = (p_0, p_1, p_2, p_3, p_4, p_5, \dots, p_{m+3})' = (\gamma, I_0, \phi^{-1}, \tau, \beta_1, \beta_2, \dots, \beta_m)'. \tag{19}$$

Notice that for the SI_KR model one has the same probabilistic model (eqn. (5) in the main text) and, therefore, the same log-posterior (eqn. (7) in the main text). The gradient of the log-posterior takes the following form

$$\frac{d\ell}{dp_i} = \begin{cases} \sum_{j=1}^n \frac{\partial \ell_{like}^j}{\partial C(t_0+j)} (s_{i,K+3}(t_0+j) - s_{i,K+3}(t_0+j-1)) + \frac{\partial \ell_{prior}}{\partial p_i} & i = 0, 1, 4, \dots, m+3, \\ \sum_{j=1}^n \frac{\partial \ell_{like}^j}{\partial p_i} + \frac{\partial \ell_{prior}}{\partial p_i} & i = 2, \\ \frac{\partial \ell_{prior}}{\partial p_i} & i = 3. \end{cases} \tag{19}$$

Additionally, we have

$$\begin{aligned}\frac{\partial \ell_{like}^j}{\partial C(t_0 + j)} &= \frac{\tilde{C}_{t_0+j}}{\eta(t_0+j)} - \frac{\tilde{C}_{t_0+j}}{\eta(t_0+j) + \phi}, \\ \frac{\partial \ell_{like}^j}{\partial p_i} &= -\delta_{i2} \left(\psi\left(\frac{\tilde{C}_{t_0+j}}{\eta(t_0+j)} + \phi\right) - \psi(\phi) + \frac{C(t_0 + j) - \frac{\tilde{C}_{t_0+j}}{\eta(t_0+j)}}{C(t_0 + j) + \phi} + \log(\phi) - \log(C(t_0 + j) + \phi) \right) \phi^2.\end{aligned}$$

The forward sensitivity analysis is characterized by the following extended system of ODEs

$$\begin{aligned}\dot{\mathbf{y}}(t) &= \mathbf{f}(t, \mathbf{y}, \mathbf{p}), \quad \mathbf{y}(t_0) = (N - p_1, p_1, 0, \dots, 0, p_1)', \\ \dot{\mathbf{s}}_i(t) &= \frac{\partial \mathbf{f}(t)}{\partial \mathbf{y}} \mathbf{s}_i(t) + \frac{\partial \mathbf{f}(t)}{\partial p_i}, \quad \mathbf{s}_i(t_0) = (-\delta_{i1}, \delta_{i1}, 0, \dots, 0, \delta_{i1})'.\end{aligned}$$

Expressions for the Jacobian matrices $\frac{\partial \mathbf{f}(t)}{\partial \mathbf{y}}$ and $\frac{\partial \mathbf{f}(t)}{\partial \mathbf{p}}$ are provided in B.2.

Appendix B Sensitivity dynamics

B.1 SE_MI_KR model

For the SE_MI_KR model described in Section Methods of the main text, differentiating the right hand sides of system (2), one obtains the following Jacobian matrix:

$$\begin{aligned}\left[\frac{\partial \mathbf{f}(t)}{\partial \mathbf{y}}\right]_{1,1} &= -\exp\left(\sum_{i=1}^m \beta_i B_i(t)\right) \frac{1}{N} \sum_{j=M+2}^{M+K+1} y_j(t), \quad \left[\frac{\partial \mathbf{f}(t)}{\partial \mathbf{y}}\right]_{2,1} = -\left[\frac{\partial \mathbf{f}(t)}{\partial \mathbf{y}}\right]_{1,1}, \quad \left[\frac{\partial \mathbf{f}(t)}{\partial \mathbf{y}}\right]_{M+K+3,1} = -\left[\frac{\partial \mathbf{f}(t)}{\partial \mathbf{y}}\right]_{1,1}, \\ \left[\frac{\partial \mathbf{f}(t)}{\partial \mathbf{y}}\right]_{j,1} &= 0, \quad 2 < j < M + K + 3, \\ \left[\frac{\partial \mathbf{f}(t)}{\partial \mathbf{y}}\right]_{i,i} &= -M\alpha, \quad \left[\frac{\partial \mathbf{f}(t)}{\partial \mathbf{y}}\right]_{i+1,i} = M\alpha, \quad \left[\frac{\partial \mathbf{f}(t)}{\partial \mathbf{y}}\right]_{j,i} = 0, \quad j \neq i, i+1, \quad i = 2, \dots, M+1, \\ \left[\frac{\partial \mathbf{f}(t)}{\partial \mathbf{y}}\right]_{1,i} &= -\exp\left(\sum_{i=1}^m \beta_i B_i(t)\right) \frac{y_1(t)}{N}, \quad \left[\frac{\partial \mathbf{f}(t)}{\partial \mathbf{y}}\right]_{2,i} = -\left[\frac{\partial \mathbf{f}(t)}{\partial \mathbf{y}}\right]_{1,i}, \quad \left[\frac{\partial \mathbf{f}(t)}{\partial \mathbf{y}}\right]_{M+K+3,i} = -\left[\frac{\partial \mathbf{f}(t)}{\partial \mathbf{y}}\right]_{1,i}, \\ \left[\frac{\partial \mathbf{f}(t)}{\partial \mathbf{y}}\right]_{i,i} &= -K\gamma, \quad \left[\frac{\partial \mathbf{f}(t)}{\partial \mathbf{y}}\right]_{i+1,i} = K\gamma, \quad \left[\frac{\partial \mathbf{f}(t)}{\partial \mathbf{y}}\right]_{j,i} = 0, \quad j \neq 1, 2, i, i+1, M+K+3 \quad i = M+2, \dots, M+K+1, \\ \left[\frac{\partial \mathbf{f}(t)}{\partial \mathbf{y}}\right]_{j,i} &= 0, \quad j = 1, \dots, M+K+3, \quad i = M+K+2, M+K+3.\end{aligned}$$

Additionally, differentiating with respect to the parameters yields

$$\begin{aligned}
\frac{\partial \mathbf{f}(t)}{\partial p_0} &= (0, -My_2(t), My_2(t) - My_3(t), \dots, My_M(t) - My_{M+1}(t), My_{M+1}(t), 0, \dots, 0), \\
\frac{\partial \mathbf{f}(t)}{\partial p_1} &= (0, \dots, 0, -Ky_{M+2}(t), Ky_{M+2}(t) - Ky_{M+3}(t), \dots, Ky_{M+K}(t) - Ky_{M+K+1}(t), Ky_{M+K+1}(t), 0), \\
\frac{\partial \mathbf{f}(t)}{\partial p_2} &= \frac{\partial \mathbf{f}(t)}{\partial p_3} = \frac{\partial \mathbf{f}(t)}{\partial p_4} = 0, \\
\frac{\partial \mathbf{f}(t)}{\partial p_i} &= \left(-\exp\left(\sum_{i=1}^m \beta_i B_i(t)\right) B_{i-4}(t) \frac{y_1(t) \sum_{j=3}^{K+2} y_j(t)}{N}, \right. \\
&\quad \exp\left(\sum_{i=1}^m \beta_i B_i(t)\right) B_{i-4}(t) \frac{y_1(t) \sum_{j=3}^{K+2} y_j(t)}{N}, 0, \dots, 0, \\
&\quad \left. \exp\left(\sum_{i=1}^m \beta_i B_i(t)\right) B_{i-4}(t) \frac{y_1(t) \sum_{j=3}^{K+2} y_j(t)}{N} \right)' \quad i = 5, \dots, m+4.
\end{aligned}$$

To compute the Hessian, a second differentiation leads to

$$\begin{aligned}
\frac{d^2 \ell}{dp_k dp_i} &= \sum_{j=1}^n \left(\frac{\partial^2 \ell_{like}^j}{\partial C^2(t_0 + j)} \frac{\partial C(t_0 + j)}{\partial p_k} \frac{\partial C(t_0 + j)}{\partial p_i} + \frac{\partial \ell_{like}^j}{\partial C(t_0 + j)} \frac{\partial^2 C(t_0 + j)}{\partial p_k \partial p_i} + \frac{\partial^2 \ell_{like}^j}{\partial p_k \partial p_i} \right) + \frac{\partial^2 \ell_{prior}}{\partial p_k \partial p_i} \\
&= \sum_{j=1}^n \left(\frac{\partial^2 \ell_{like}^j}{\partial C^2(t_0 + j)} \left(\frac{\partial C_I(t_0 + j)}{\partial p_k} - \frac{\partial C_I(t_0 + j - 1)}{\partial p_k} \right) \left(\frac{\partial C_I(t_0 + j)}{\partial p_i} - \frac{\partial C_I(t_0 + j - 1)}{\partial p_i} \right) \right) \\
&\quad + \frac{\partial \ell_{like}^j}{\partial C(t_0 + j)} \left(\frac{\partial^2 C_I(t_0 + j)}{\partial p_k \partial p_i} - \frac{\partial^2 C_I(t_0 + j - 1)}{\partial p_k \partial p_i} \right) + \frac{\partial^2 \ell_{like}^j}{\partial p_k \partial p_i} + \frac{\partial^2 \ell_{prior}}{\partial p_k \partial p_i}.
\end{aligned}$$

Defining the second order sensibilities as

$$\mathbf{s}_i^k(t) = \frac{\partial^2 \mathbf{y}(t)}{\partial p_k \partial p_i} = \left(\frac{\partial^2}{\partial p_k \partial p_i} y_1(t), \dots, \frac{\partial^2}{\partial p_k \partial p_i} y_{M+K+1}(t) \right)' = (s_{i,1}^k(t), \dots, s_{i,M+K+1}^k(t)),$$

one gets the following ODEs

$$\dot{\mathbf{s}}_{i,j}^k(t) = \frac{\partial^2 \mathbf{f}_j(t)}{\partial \mathbf{y}^2} \mathbf{s}_k(t) \mathbf{s}_i(t) + \frac{\partial \mathbf{f}_j(t)}{\partial \mathbf{y}} \mathbf{s}_i^k(t) + \frac{\partial^2 \mathbf{f}_j(t)}{\partial p_k \partial p_i}, \quad \mathbf{s}_i^k(t_0) = \mathbf{0}.$$

Hence the Hessian can be computed by solving the extended ODE system

$$\begin{aligned}
\dot{\mathbf{y}}(t) &= \mathbf{f}(t, \mathbf{y}, \mathbf{p}), \quad \mathbf{y}(t_0) = (N - p_2, p_2, 0, \dots, 0, p_2)', \\
\dot{\mathbf{s}}_i(t) &= \frac{\partial \mathbf{f}(t)}{\partial \mathbf{y}} \mathbf{s}_i(t) + \frac{\partial \mathbf{f}(t)}{\partial p_i}, \quad \mathbf{s}_i(t_0) = (-\delta_{i2}, \delta_{i2}, 0, \dots, 0, \delta_{i2})', \\
\dot{\mathbf{s}}_{i,j}^k(t) &= \frac{\partial^2 \mathbf{f}_j(t)}{\partial \mathbf{y}^2} \mathbf{s}_k(t) \mathbf{s}_i(t) + \frac{\partial \mathbf{f}_j(t)}{\partial \mathbf{y}} \mathbf{s}_i^k(t) + \frac{\partial^2 \mathbf{f}_j(t)}{\partial p_k \partial p_i}, \quad \mathbf{s}_{i,j}^k(t_0) = 0, j = 1, \dots, M + K + 1.
\end{aligned} \tag{20}$$

B.2 SI_KR model

For the SI_KR model described in A, differentiating the right hand sides of system (17), one obtains the following Jacobian matrix:

$$\begin{aligned}
\left[\frac{\partial \mathbf{f}(t)}{\partial \mathbf{y}} \right]_{1,1} &= -\exp\left(\sum_{i=1}^m \beta_i B_i(t)\right) \frac{1}{N} \sum_{j=2}^{K+1} y_j(t), \quad \left[\frac{\partial \mathbf{f}(t)}{\partial \mathbf{y}} \right]_{2,1} = -\left[\frac{\partial \mathbf{f}(t)}{\partial \mathbf{y}} \right]_{1,1}, \quad \left[\frac{\partial \mathbf{f}(t)}{\partial \mathbf{y}} \right]_{K+3,1} = -\left[\frac{\partial \mathbf{f}(t)}{\partial \mathbf{y}} \right]_{1,1}, \\
\left[\frac{\partial \mathbf{f}(t)}{\partial \mathbf{y}} \right]_{j,1} &= 0, \quad 2 < j < K+3, \\
\left[\frac{\partial \mathbf{f}(t)}{\partial \mathbf{y}} \right]_{1,2} &= -\exp\left(\sum_{i=1}^m \beta_i B_i(t)\right) \frac{y_1(t)}{N}, \quad \left[\frac{\partial \mathbf{f}(t)}{\partial \mathbf{y}} \right]_{2,2} = -\left[\frac{\partial \mathbf{f}(t)}{\partial \mathbf{y}} \right]_{1,2} - K\gamma, \quad \left[\frac{\partial \mathbf{f}(t)}{\partial \mathbf{y}} \right]_{K+3,2} = -\left[\frac{\partial \mathbf{f}(t)}{\partial \mathbf{y}} \right]_{1,2}, \\
\left[\frac{\partial \mathbf{f}(t)}{\partial \mathbf{y}} \right]_{3,2} &= K\gamma, \quad \left[\frac{\partial \mathbf{f}(t)}{\partial \mathbf{y}} \right]_{j,2} = 0, \quad 3 < j < K+3, \\
\left[\frac{\partial \mathbf{f}(t)}{\partial \mathbf{y}} \right]_{1,i} &= -\exp\left(\sum_{i=1}^m \beta_i B_i(t)\right) \frac{y_1(t)}{N}, \quad \left[\frac{\partial \mathbf{f}(t)}{\partial \mathbf{y}} \right]_{2,i} = -\left[\frac{\partial \mathbf{f}(t)}{\partial \mathbf{y}} \right]_{1,i}, \quad \left[\frac{\partial \mathbf{f}(t)}{\partial \mathbf{y}} \right]_{K+3,i} = -\left[\frac{\partial \mathbf{f}(t)}{\partial \mathbf{y}} \right]_{1,i}, \\
\left[\frac{\partial \mathbf{f}(t)}{\partial \mathbf{y}} \right]_{i,i} &= -K\gamma, \quad \left[\frac{\partial \mathbf{f}(t)}{\partial \mathbf{y}} \right]_{i+1,i} = K\gamma, \quad \left[\frac{\partial \mathbf{f}(t)}{\partial \mathbf{y}} \right]_{j,i} = 0, \quad j \neq 1, 2, i, i+1, K+3 \quad i = 3, \dots, K+1, \\
\left[\frac{\partial \mathbf{f}(t)}{\partial \mathbf{y}} \right]_{j,i} &= 0, \quad j = 1, \dots, K+3, \quad i = K+2, K+3.
\end{aligned}$$

The Jacobian with respect to the parameters is characterized by

$$\begin{aligned}
\frac{\partial \mathbf{f}}{\partial p_0}(t) &= (0, -Ky_2(t), Ky_2(t) - Ky_3(t), \dots, Ky_K(t) - Ky_{K+1}(t), Ky_{K+1}(t), 0), \\
\frac{\partial \mathbf{f}}{\partial p_1}(t) &= \frac{\partial \mathbf{f}}{\partial p_2}(t) = \frac{\partial \mathbf{f}}{\partial p_3}(t) = 0, \\
\frac{\partial \mathbf{f}}{\partial p_i}(t) &= \left(-\exp\left(\sum_{i=1}^m \beta_i B_i(t)\right) B_{i-4}(t) \frac{y_1(t) \sum_{j=2}^{K+1} y_j(t)}{N}, \right. \\
&\quad \left. \exp\left(\sum_{i=1}^m \beta_i B_i(t)\right) B_{i-4}(t) \frac{y_1(t) \sum_{j=2}^{K+1} y_j(t)}{N}, 0, \dots, 0, \right. \\
&\quad \left. \exp\left(\sum_{i=1}^m \beta_i B_i(t)\right) B_{i-4}(t) \frac{y_1(t) \sum_{j=2}^{K+1} y_j(t)}{N} \right)' \quad i = 4, \dots, m+3.
\end{aligned}$$

Appendix C SIR/SEIR-like models with a diffusion-based transmission rate

Using the ideas in [16], we provide stochastic ordinary differential equations (SODEs) for $SE_M I_K R$ and $SI_K R$ models, where $\log \beta(t)$ is governed by a diffusion process. An additional parameter β_0 to model the initial transmission rate is introduced.

In this setting, the $SE_M I_K R$ equations become

$$\begin{aligned}
\frac{dS(t)}{dt} &= -\beta_0\beta(t)S(t)\frac{\sum_{j=1}^K I_j(t)}{N} = -\beta_0\beta(t)S(t)\frac{I(t)}{N}, \\
\frac{dE_1(t)}{dt} &= \beta_0\beta(t)S(t)\frac{I(t)}{N} - M\alpha E_1(t), \\
\frac{dE_2(t)}{dt} &= M\alpha E_1(t) - M\alpha E_2(t), \\
&\dots, \\
\frac{dE_M(t)}{dt} &= M\alpha E_{M-1}(t) - M\alpha E_M(t), \\
\frac{dI_1(t)}{dt} &= M\alpha E_M(t) - K\gamma I_1(t), \\
\frac{dI_2(t)}{dt} &= K\gamma I_1(t) - K\gamma I_2(t), \\
&\dots, \\
\frac{dI_K(t)}{dt} &= K\gamma I_{K-1}(t) - K\gamma I_K(t), \\
\frac{dR(t)}{dt} &= \frac{d}{dt}(N - S(t) - E(t) - I(t)) = K\gamma I_K(t), \\
\frac{dC_I(t)}{dt} &= \beta_0\beta(t)S(t)\frac{I(t)}{N}, \\
\frac{d\log \beta(t)}{dt} &= \sigma dB(t),
\end{aligned} \tag{21}$$

with initial conditions:

$$\begin{aligned}
S(t_0) &= N - E_0, E_1(t_0) = E_0, \\
E_2(t_0) &= \dots = E_M(t_0) = I_1(t_0) = \dots = I_K(t_0) = 0, \\
R(t_0) &= 0, C_I(t_0) = E_0, \beta(t_0) = 1,
\end{aligned}$$

where $B(t)$ denotes the Standard Brownian Motion.

The parameters of interest for model (5) in the main text, based on the dynamics (21) are

$$\mathbf{p} = (p_0, p_1, p_2, p_3, p_4, p_5, p_6)' = (\alpha, \gamma, E_0, \phi^{-1}, \beta_0, \sigma)'.$$

The SODEs corresponding to the SI_KR model are

$$\begin{aligned}
\frac{dS(t)}{dt} &= -\beta_0\beta(t)S(t)\frac{\sum_{j=1}^K I_j(t)}{N} = -\beta_0\beta(t)S(t)\frac{I(t)}{N}, \\
\frac{dI_1(t)}{dt} &= \beta_0\beta(t)S(t)\frac{I(t)}{N} - K\gamma I_1(t), \\
\frac{dI_2(t)}{dt} &= K\gamma I_1(t) - K\gamma I_2(t), \\
&\dots, \\
\frac{dI_K(t)}{dt} &= K\gamma I_{K-1}(t) - K\gamma I_K(t), \\
\frac{dR(t)}{dt} &= \frac{d}{dt}(N - S(t) - I(t)) = K\gamma I_K(t), \\
\frac{dC_I(t)}{dt} &= \beta_0\beta(t)S(t)\frac{I(t)}{N}, \\
\frac{d\log \beta(t)}{dt} &= \sigma dB(t),
\end{aligned} \tag{22}$$

with initial conditions:

$$S(t_0) = N - I_0, I(t_0) = I_1(t_0) = I_0, R(t_0) = 0, C_I(t_0) = I_0, \beta(t_0) = 1.$$

The corresponding parameters to estimate are

$$\mathbf{p} = (p_0, p_1, p_2, p_3, p_4, p_5)' = (\gamma, I_0, \phi^{-1}, \beta_0, \sigma)'$$

The parameter estimation for these models is performed using a type of Particle Filter Monte Carlo, known as SMC² [11] and implemented in the R-package `rbi` [27] (see [43] for implementation ideas).

Appendix D Generalized Hamiltonian Monte Carlo

The common class of separable Hamiltonian systems is characterized by a separable Hamiltonian $H(\mathbf{p}, \mathbf{q}) = U(\mathbf{p}) + K(\mathbf{q})$. Here, \mathbf{p} is the position, \mathbf{q} is the momentum, $U(\mathbf{p})$ and $K(\mathbf{q})$ are the potential and kinetic energies, respectively. The equations governing the motion of the system are the Hamiltonian equations

$$\begin{aligned}
\frac{d\mathbf{p}}{dt} &= \nabla_{\mathbf{q}}H(\mathbf{p}, \mathbf{q}) = \nabla_{\mathbf{q}}K(q) \\
\frac{d\mathbf{q}}{dt} &= -\nabla_{\mathbf{p}}H(\mathbf{p}, \mathbf{q}) = -\nabla_{\mathbf{p}}U(\mathbf{p}).
\end{aligned}$$

Solving a system analytically or numerically, with a symplectic method Ψ_t , evolves the system from its original position and momentum $(\mathbf{p}(t_0), \mathbf{q}(t_0))$, to the corresponding values at a time $t_0 + t$, $\Psi_t(\mathbf{p}(t_0), \mathbf{q}(t_0)) = (\mathbf{p}(t_0 + t), \mathbf{q}(t_0 + t))$. Though Hamiltonian dynamics was formulated for Physics it is applicable to many continuous state problems due to its useful properties, such as conservation of the Hamiltonian, volume preservation and reversibility. In non-physical applications,

a variable/parameter of interest plays a role of ‘position’ \mathbf{p} whereas ‘momentum’ \mathbf{q} is an auxiliary vector introduced artificially. Potential energy $U(\mathbf{p})$ is simply minus the log-posterior distribution, i.e. $-\ell(\mathbf{p})$.

The canonical distribution is the link between Hamiltonian dynamics and Markov Chain Monte Carlo (MCMC) - two constituents of a Hamilton Monte Carlo method (HMC). Loosely speaking it describes the probability of a system in a thermal bath to be at (\mathbf{p}, \mathbf{q}) when the temperature is T . The exact expression is the following (Z is the normalizing constant):

$$P(\mathbf{p}, \mathbf{q}) = \frac{1}{Z} e^{-H(\mathbf{p}, \mathbf{q})/T} = \frac{1}{Z} e^{-U(\mathbf{p})/T} e^{K(\mathbf{q})/T}.$$

Taking $T = 1$ and $U(\mathbf{p}) = -\ell(\mathbf{p})$ one gets

$$P(\mathbf{p}, \mathbf{q}) = \text{prior}(\mathbf{p}) L(\mathbf{p} | \tilde{C}) \frac{1}{Z} e^{-K(\mathbf{q})} = \text{posterior}(\mathbf{p}) \frac{1}{Z} e^{-K(\mathbf{q})}.$$

Therefore, Hamiltonian-based Monte Carlo methods sample with MCMC from the joint target distribution $P(\mathbf{p}, \mathbf{q})$, using Hamiltonian dynamics as mechanism for making a new proposal and the Metropolis test for accepting/rejecting such a proposal. Further details can be found in [44] and references therein.

In this work we use a generalized formulation of Hamiltonian Monte Carlo, i.e. Generalized Hamiltonian (Hybrid) Monte Carlo (GHMC) [28]. In contrast to HMC, where a momentum is completely reset for each new proposal, GHMC introduces a partial momentum update

$$(\mathbf{q}^*, \mathbf{u}^*) = \begin{pmatrix} \sqrt{1-\psi} & \sqrt{\psi} \\ -\sqrt{\psi} & \sqrt{1-\psi} \end{pmatrix} \begin{pmatrix} \mathbf{q}^* \\ \mathbf{u} \end{pmatrix}$$

with $0 < \psi \leq 1$ and $\mathbf{u} \sim N(0, \mathbf{M})$.

Otherwise, like a standard HMC, GHMC generates a proposal $\Psi_t(\mathbf{p}(0), \mathbf{q}(0))$, performs the Metropolis test, i.e. accept $(\mathbf{p}^*, \mathbf{q}^*) = \Psi_t(\mathbf{p}(0), \mathbf{q}(0))$ with the probability

$$\text{accep_prob} = \min\{1, e^{-(H(\Psi_t(\mathbf{p}(0), \mathbf{q}(0))) - H(\mathbf{p}(0), \mathbf{q}(0)))}\}.$$

However, if a proposal is rejected, a moment flip is applied to a next proposal before a partial momentum update: $(\mathbf{p}^*, \mathbf{q}^*) = (\mathbf{p}(0), -\mathbf{q}(0))$ in order to satisfy a detailed balance condition.

Notice that a standard HMC is a special case of GHMC and it can be recovered by setting $\psi = 1$ in the partial update step of GHMC.

Appendix E Monte Carlo Detailed Results

In this section further details and results of the experiments carried out in Section Results and discussion of the main text are presented. Mainly, trace plots and posterior densities of the epidemiologically relevant parameters are provided.

E.1 Case study 1: Synthetic data

E.1.1 Additional plots

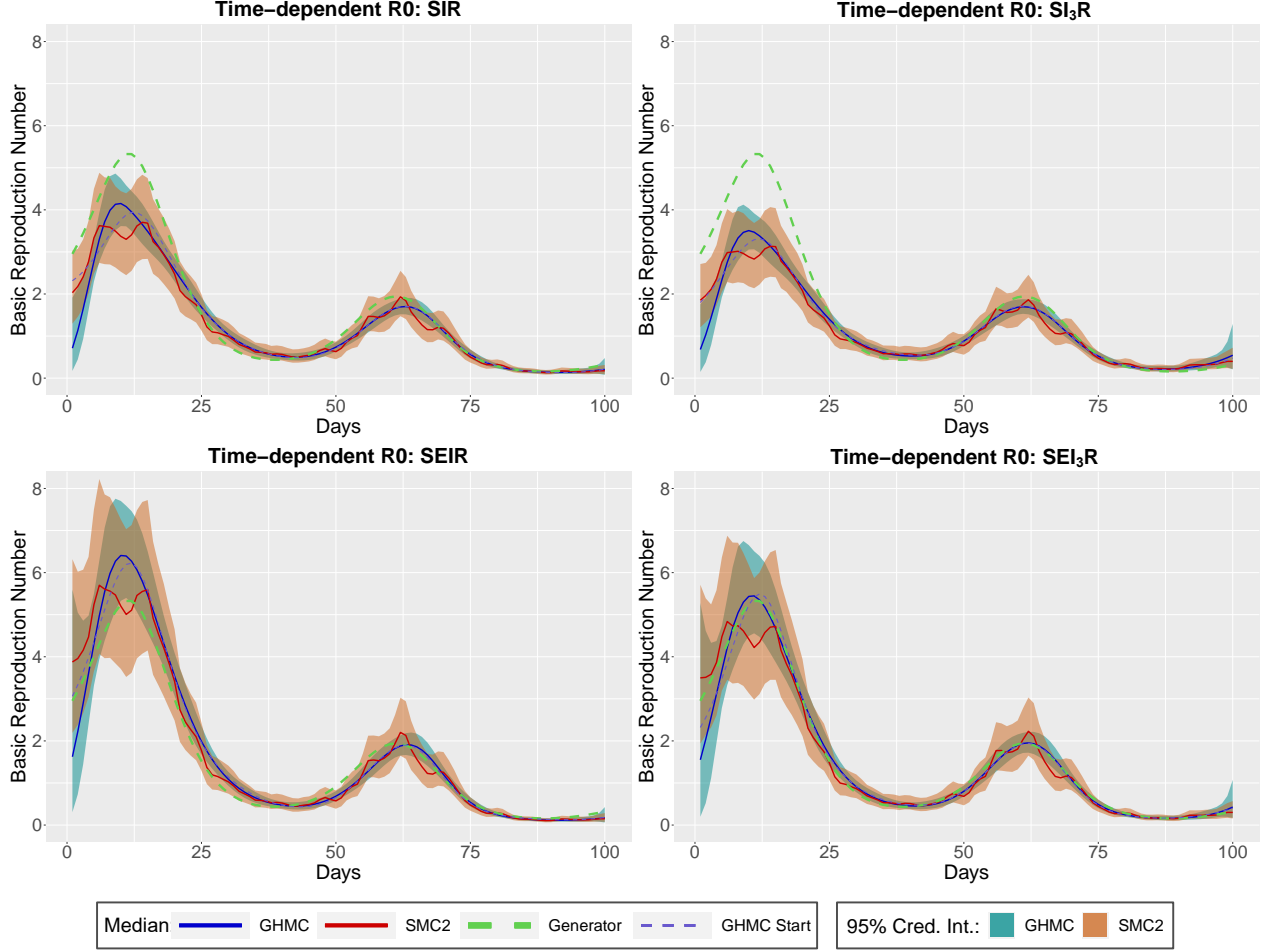


Figure 7: For the synthetic data: posterior medians (solid lines) and 95% credible intervals (shaded areas) of the time-dependent basic reproduction number, $R_0(t) = \beta(t)/\gamma$, for a spline-based dynamics sampled with GHMC (combination of 10 chains with 10000 production steps) and a diffusion-based dynamics sampled with SMC²(combination of 5 chains with 700 particles and 1000 production steps). Four different compartmental models SIR, SI₃R, SEIR and SEI₃R are displayed. Dashed purple lines represent the starting values of the GHMC chains corresponding to the result of the tuning step in Algorithm 1 in the main text. Dashed green lines show the corresponding values of the true generator \mathbf{p}^{syn} (see (14) in the main text).

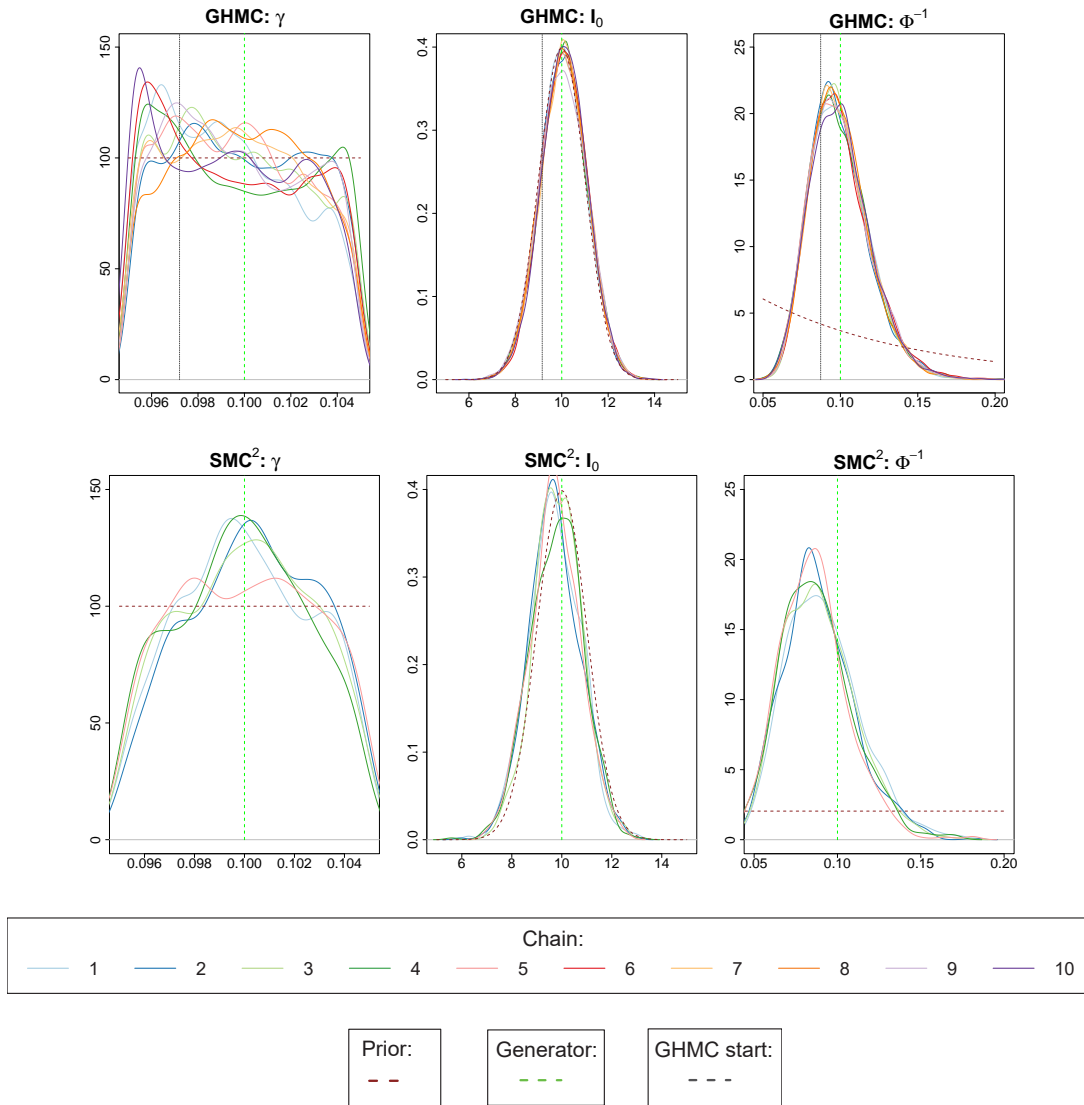


Figure 8: For the synthetic data: parameters' posterior densities for GHMC (top row) and SMR² (bottom row) corresponding to top-left of Figure 2 (main text) and Figure 7 (SIR model). Dashed green vertical lines correspond to the true values.

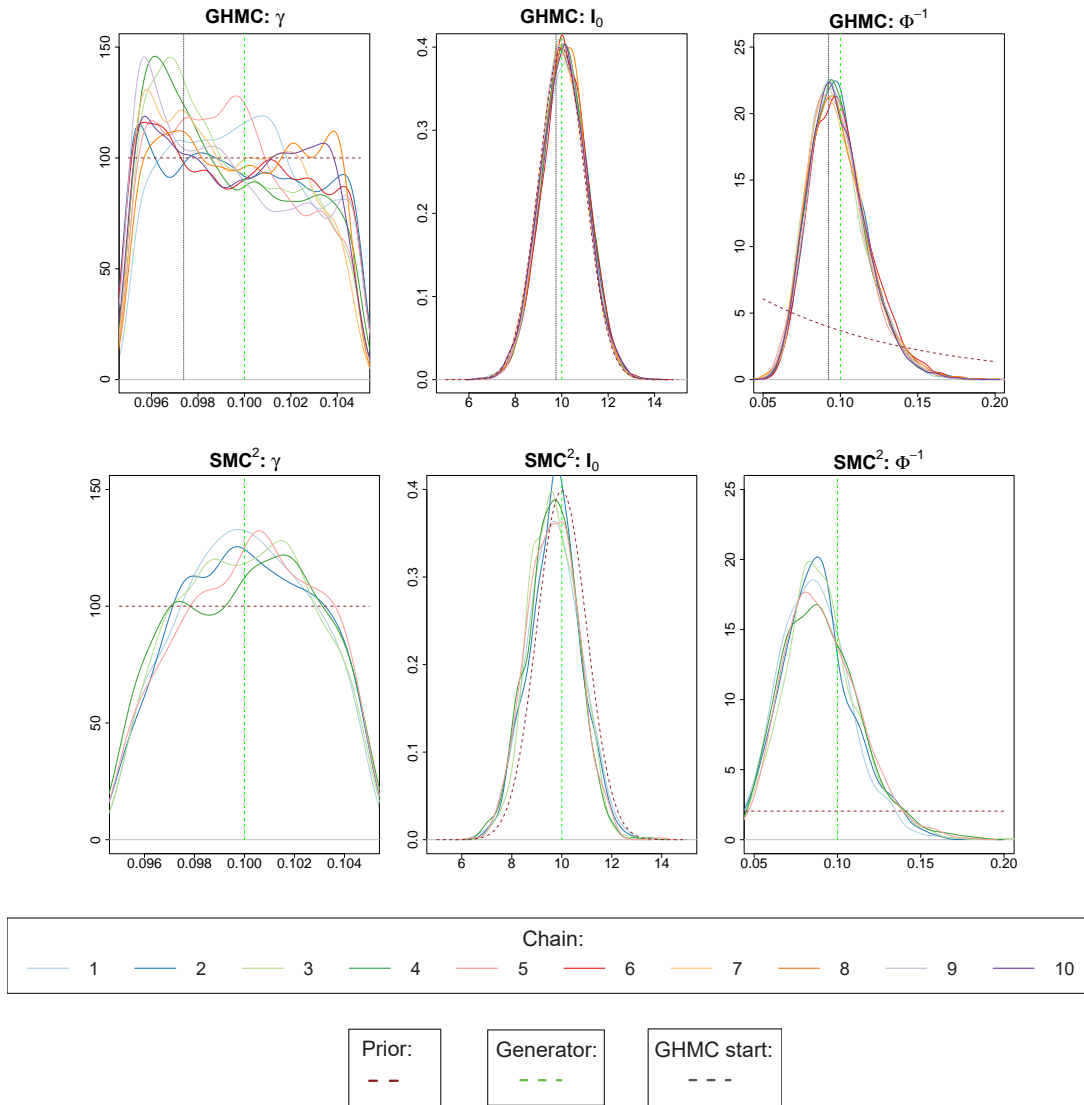


Figure 9: For the synthetic data: parameters' posterior densities for GHMC (top row) and SMR² (bottom row) corresponding to top-right of Figure 2 (main text) and Figure 7 (SI₃R model). Dashed green vertical lines correspond to the true values.

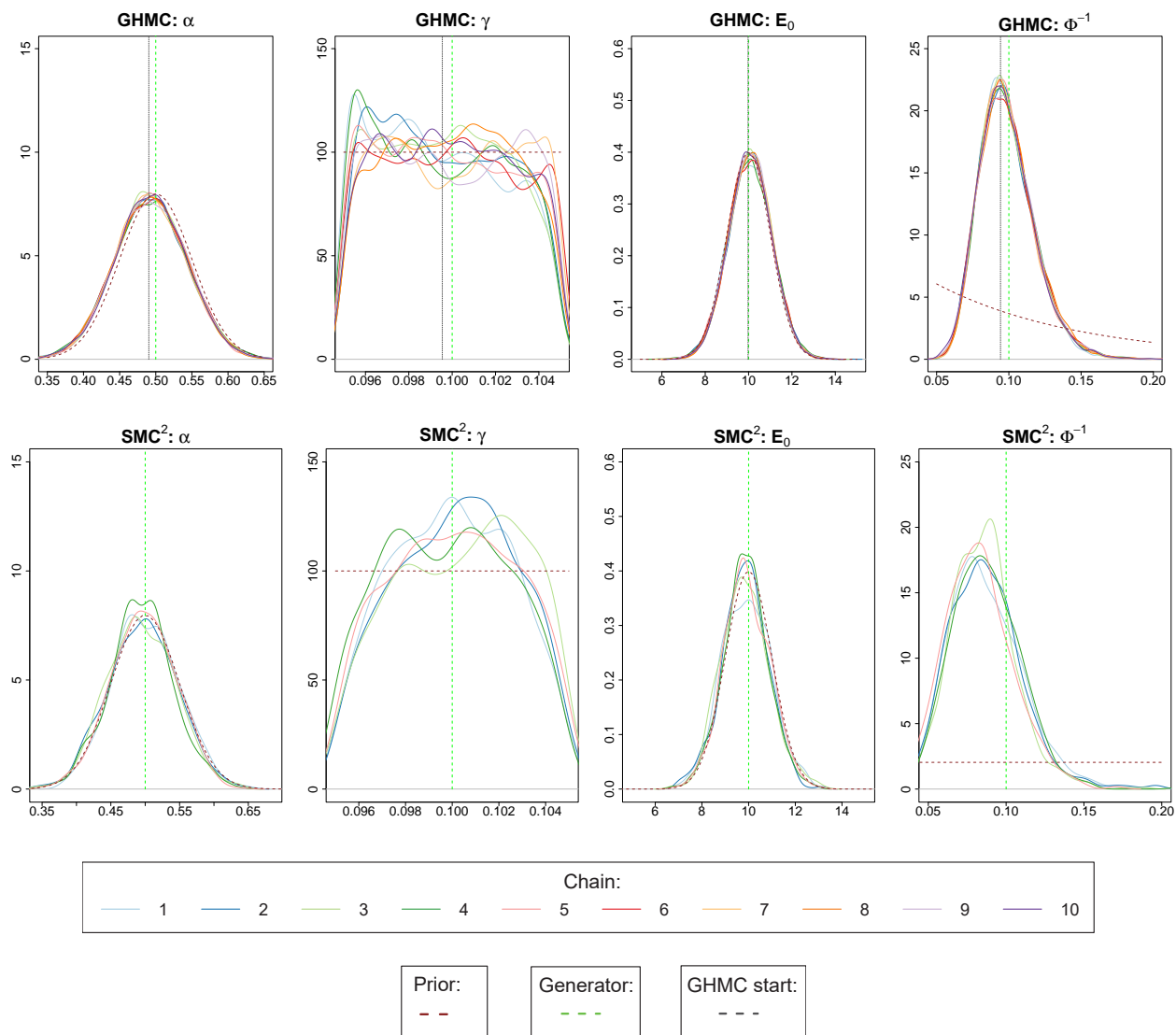


Figure 10: For the synthetic data: parameters' posterior densities for GHMC (top row) and SMR² (bottom row) corresponding to bottom-left of Figure 2 (main text) and Figure 7 (SEIR model). Dashed green vertical lines correspond to the true values.

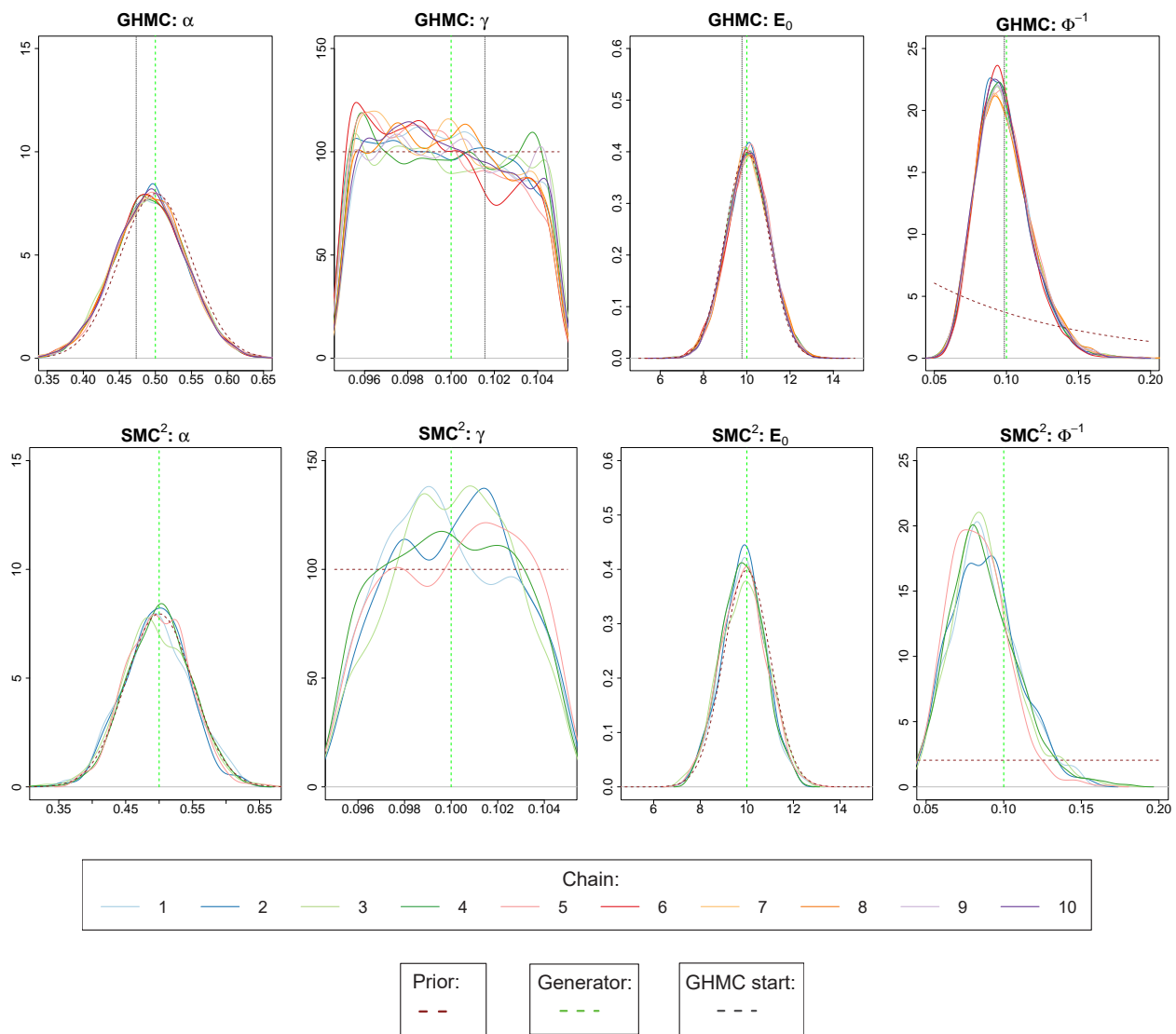


Figure 11: For the synthetic data: parameters' posterior densities for GHMC (top row) and SMR² (bottom row) corresponding to bottom-right of Figure 2 (main text) and Figure 7 (SEI₃R model). Dashed green vertical lines correspond to the true values.

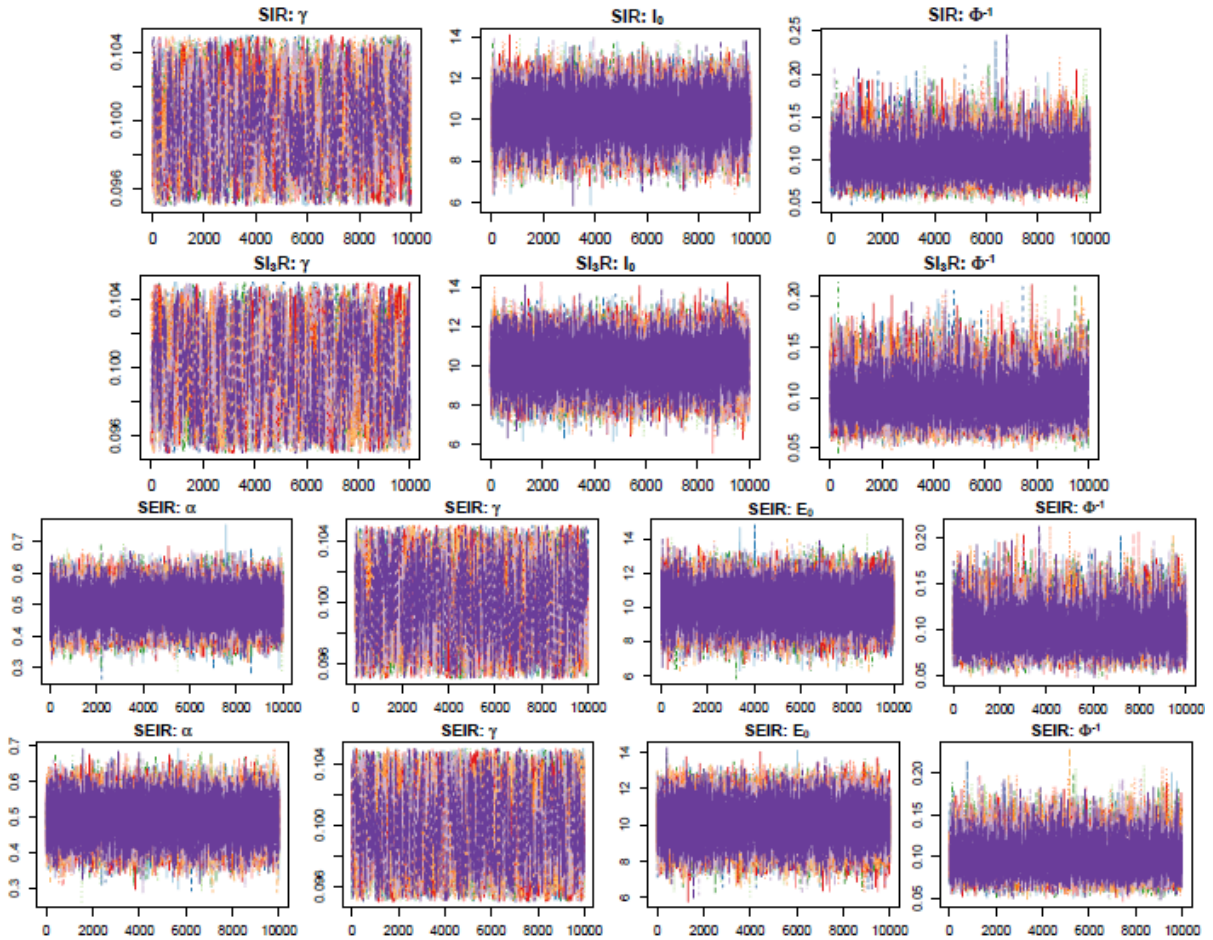


Figure 12: For the synthetic data: trace-plot of the epidemiologically relevant variables for 10 chains of GHMC for the models corresponding to Figure 2 (main text).

E.1.2 A different prior on γ

In this section we provide the results of applying the same procedure described in Section Case study 1: Synthetic data of the main text, but with the following choice of priors for HMC

$$\begin{aligned} \alpha_{HMC} &\sim N(0.5, 0.05^2), & \gamma_{HMC} &\sim N(0.1, 0.05^2), \\ E_{0,HMC} &\sim N(10, 1), & I_{0,HMC} &\sim N(10, 1), \\ \phi_{HMC}^{-1} &\sim Exp(10), & \tau_{HMC} &\sim InverseGamma(1, 0.005), \end{aligned} \quad (23)$$

and SMC²

$$\begin{aligned} \alpha_{SMC^2} &\sim \alpha_{HMC}, & \gamma_{SMC^2} &\sim \gamma_{HMC}, & E_{0,SMC^2} &\sim E_{0,HMC}, & I_{0,SMC^2} &\sim I_{0,HMC} \\ \phi_{SMC^2}^{-1} &\sim U(0.01, 0.5), & \sigma_{SMC^2} &\sim U(0.01, 1), & \beta_{0,SMC^2} &\sim U(0.1, 1). \end{aligned} \quad (24)$$

In both cases, we used a much less informative prior on γ than the one considered in the main text.

From Figure 13, one can see that all models with both samplers describe the data well and, furthermore, the results are almost indistinguishable from the ones shown in Figure 2 of the main text.

Things are different for the transmission-rate shown in Figure 14. A noticeable distinction can be observed on the second wave (after 45 days), where the posterior median of the transmission rate for the spline-based dynamic model is lower than the one for the diffusion-based model. Such a difference in behavior, however, is not reflected in the posterior predictive checks on daily incidence (see Figure 13). A cause of such behaviour is the different nature of the sampling procedures which makes the prior on γ for GHMC much less restrictive than for SMC². This allows for the values of γ explored by GHMC to be significantly lower than those observed with SMC² (see Figures 16-19), and γ is strongly correlated with the transmission rate $\beta(t)$. More precisely, a large number of new reported cases can be explained, in terms of the dynamics, by a high transmission rate, but also by a large recovery time (small value for γ). This is clearly seen when one depicts the basic reproduction number, $R_0(t) = \beta(t)/\gamma$, as in Figure 15. Now all models, for both samplers, contain the generator's R_0 and the respective posterior medians are close to its value.

Comparing Figure 15 and Figure 7, one can see that allowing for more freedom in γ allows for much greater uncertainty in the basic reproduction number.

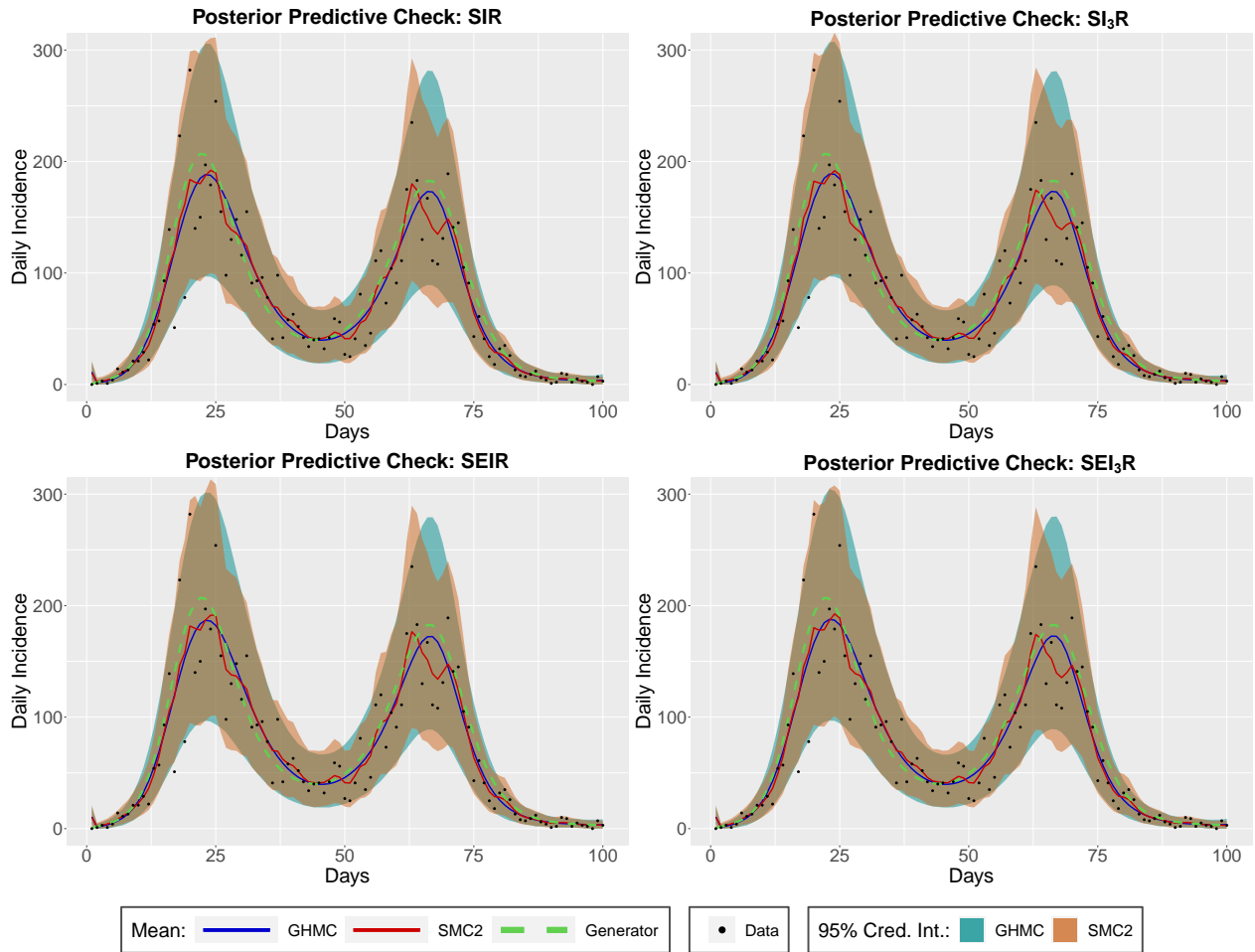


Figure 13: For the synthetic data: posterior predictive checks on daily incidence for a spline-based dynamics sampled with GHMC (combination of 10 chains with 10000 production steps) and a diffusion-based dynamics sampled with SMC²(combination of 5 chains with 700 particles and 1000 production steps) for four different compartmental models SIR, SI₃R, SEIR and SEI₃R. Dashed green lines represent the corresponding values of the true generator \mathbf{p}^{syn} (see (14) in the main text).

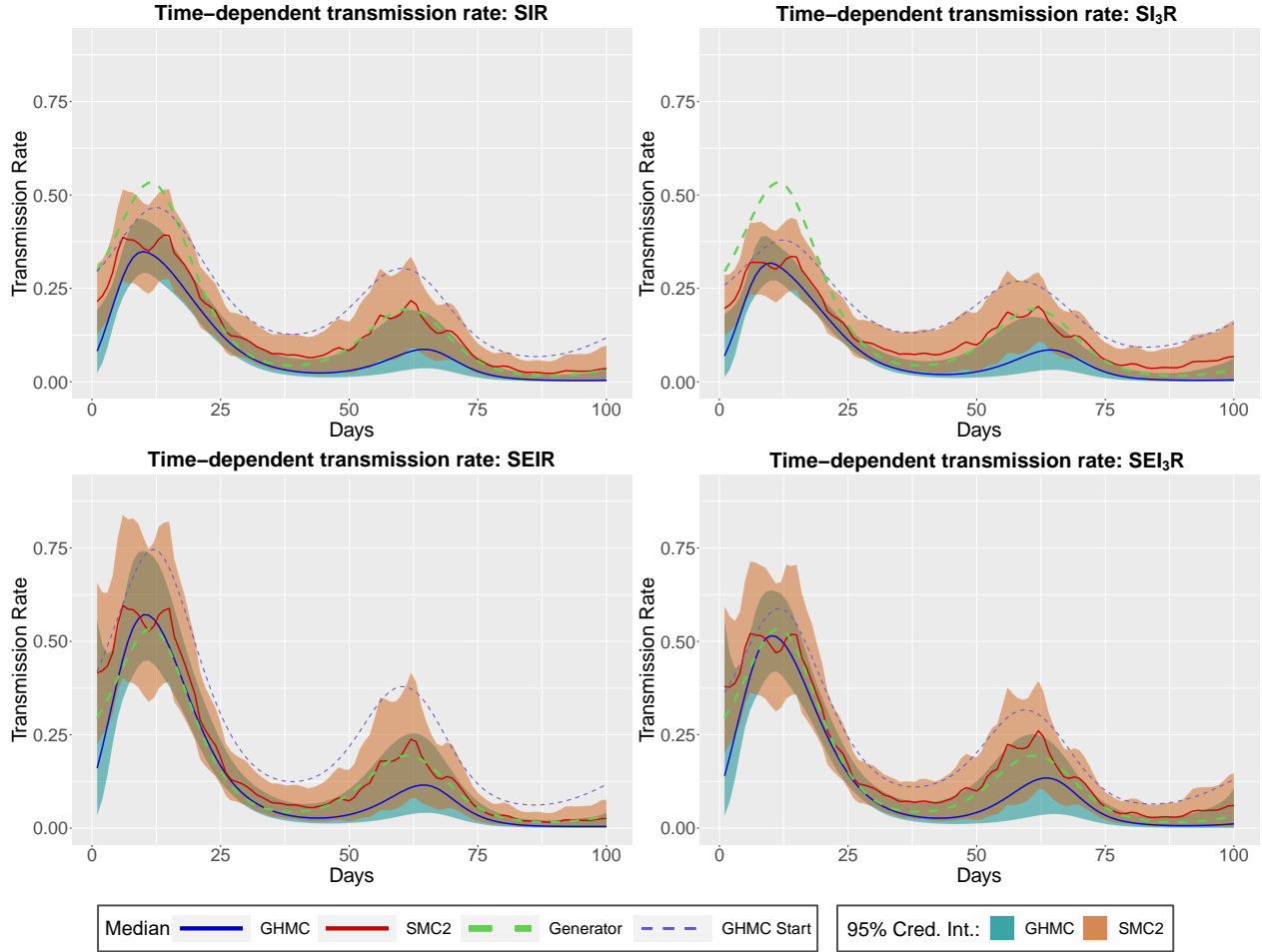


Figure 14: For the synthetic data: posterior medians (solid lines) and 95% credible intervals (shaded areas) of the time-dependent transmission rate, $\beta(t)$, for a spline-based dynamics sampled with GHMC (combination of 10 chains with 10000 production steps) and a diffusion-based dynamics sampled with SMC²(combination of 5 chains with 700 particles and 1000 production steps) for four different compartmental models SIR, SI_3R , SEIR and SEI_3R . Dashed purple lines represent the starting values of the GHMC chains corresponding to the result of the tuning step in Algorithm 1 in the main text. Dashed green shows the corresponding values of the true generator \mathbf{p}^{syn} (see (14) in the main text).

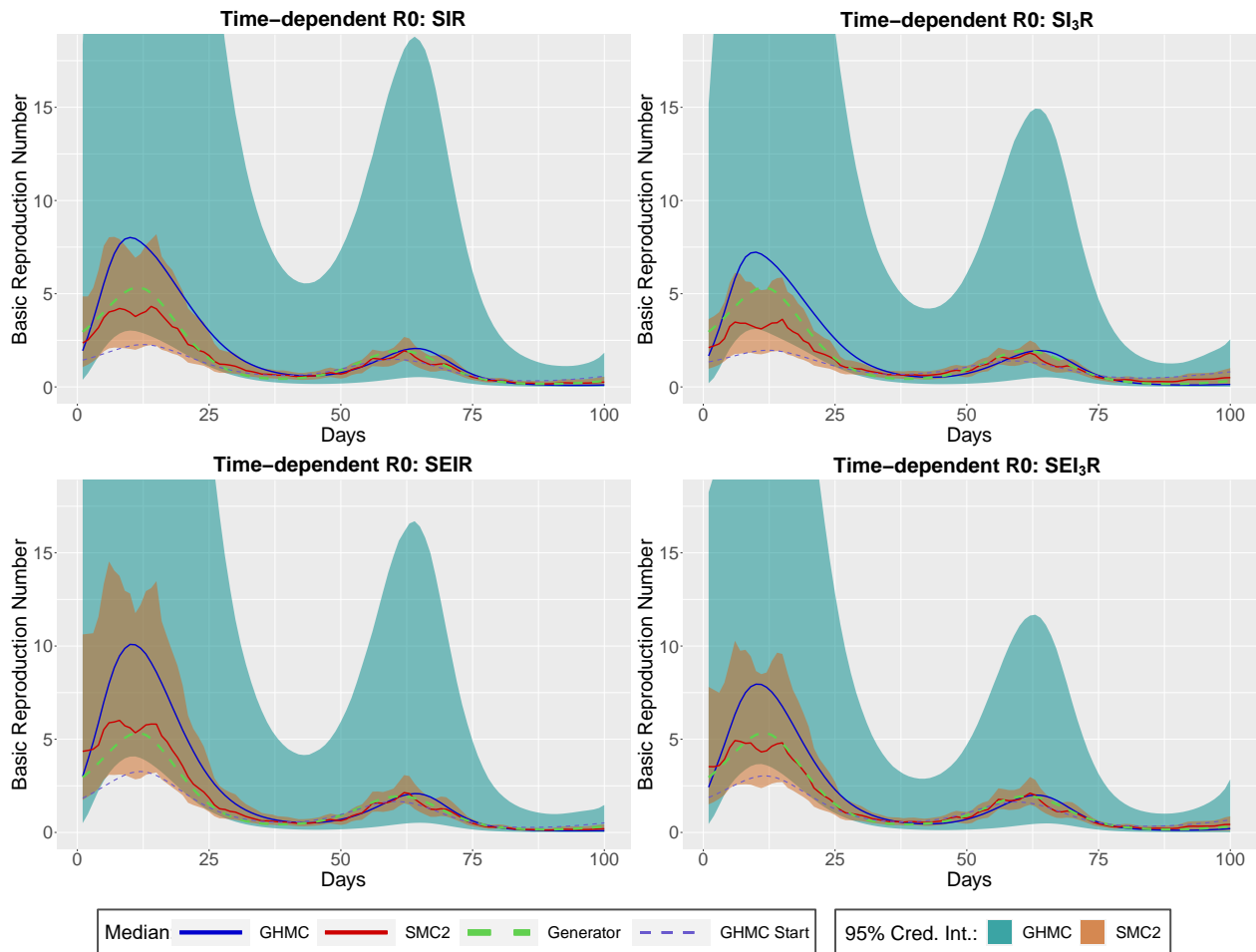


Figure 15: For the synthetic data: posterior medians (solid lines) and 95% credible intervals (shaded areas) of the time-dependent basic reproduction number, $R_0(t) = \beta(t)/\gamma$, for a spline-based dynamics sampled with GHMC (combination of 10 chains with 10000 production steps) and a diffusion-based dynamics sampled with SMC²(combination of 5 chains with 700 particles and 1000 production steps). Four different compartmental models SIR, SI_3R , SEIR and SEI_3R are displayed. Dashed purple lines represent the starting values of the GHMC chains corresponding to the result of the tuning step in Algorithm 1 in the main text. Dashed green lines show the corresponding values of the true generator \mathbf{p}^{syn} (see (14) in the main text).

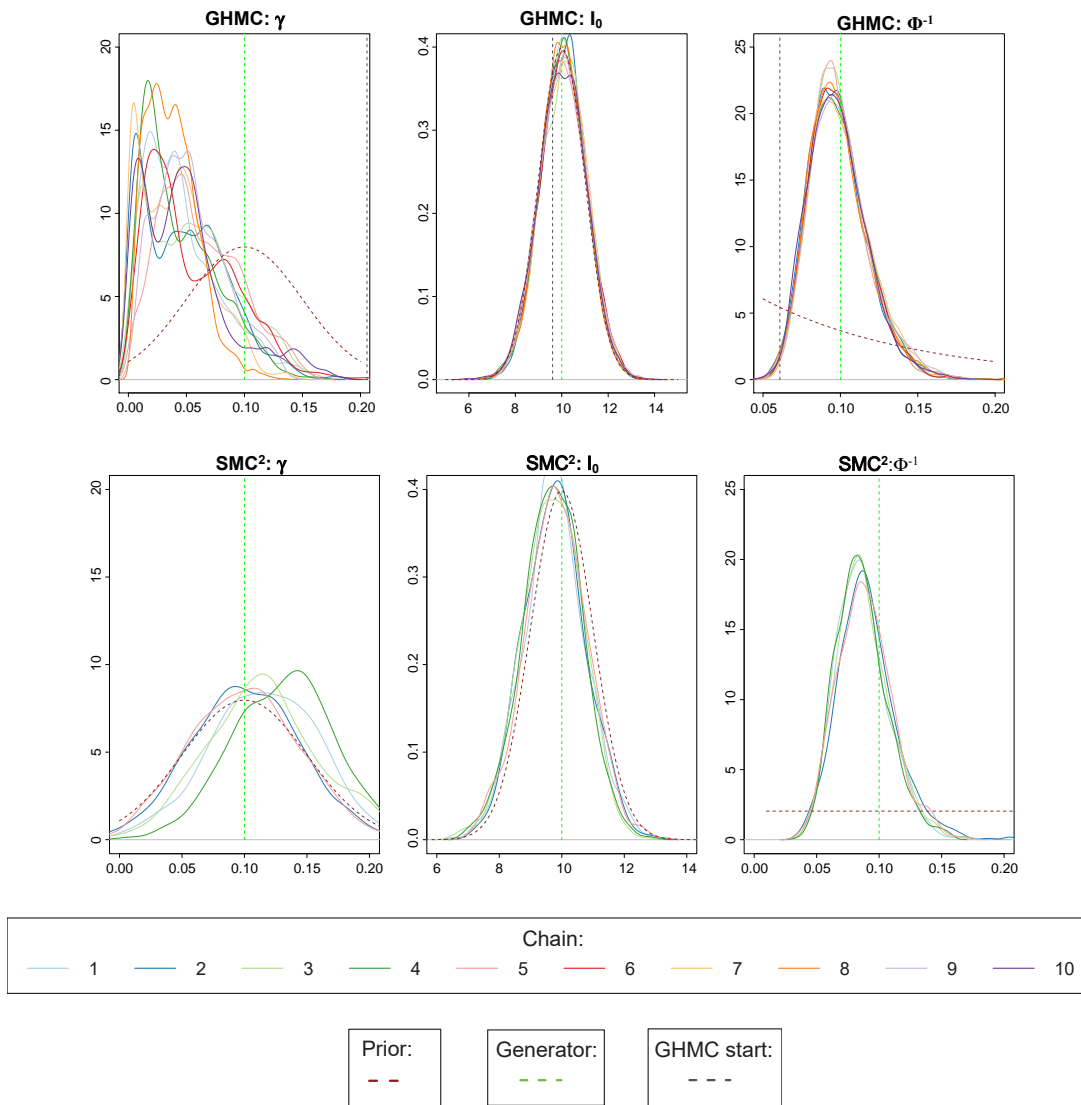


Figure 16: For the synthetic data: parameters' posterior densities for GHMC (top row) and SMR² (bottom row) corresponding to top-left of Figures 13 and 15 (SIR model). Dashed green vertical lines correspond to the true values.

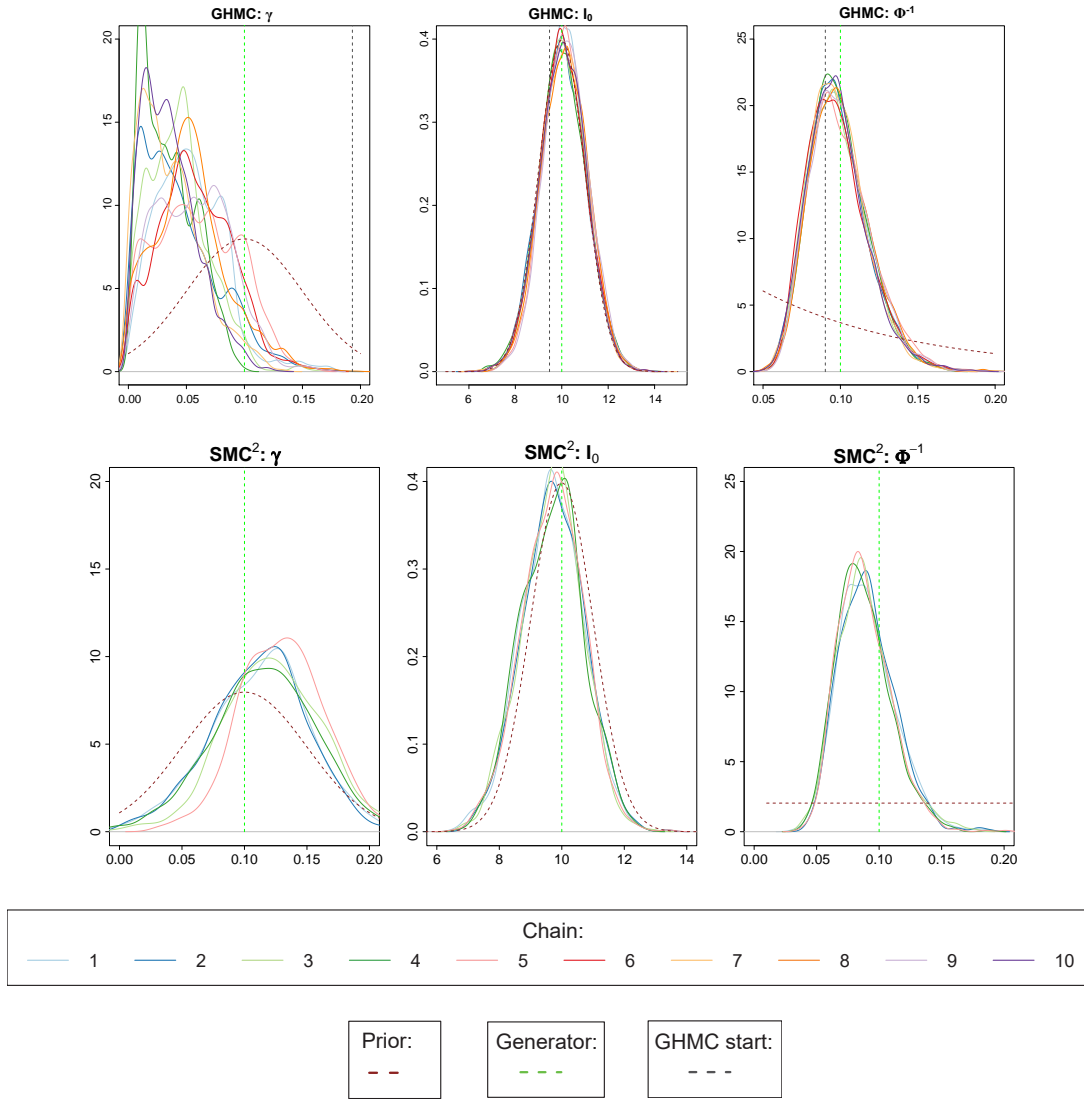


Figure 17: For the synthetic data: parameters' posterior densities for GHMC (top row) and SMR² (bottom row) corresponding to top-right of Figures 13 and 15 (SI₃R model). Dashed green vertical lines correspond to the true values.

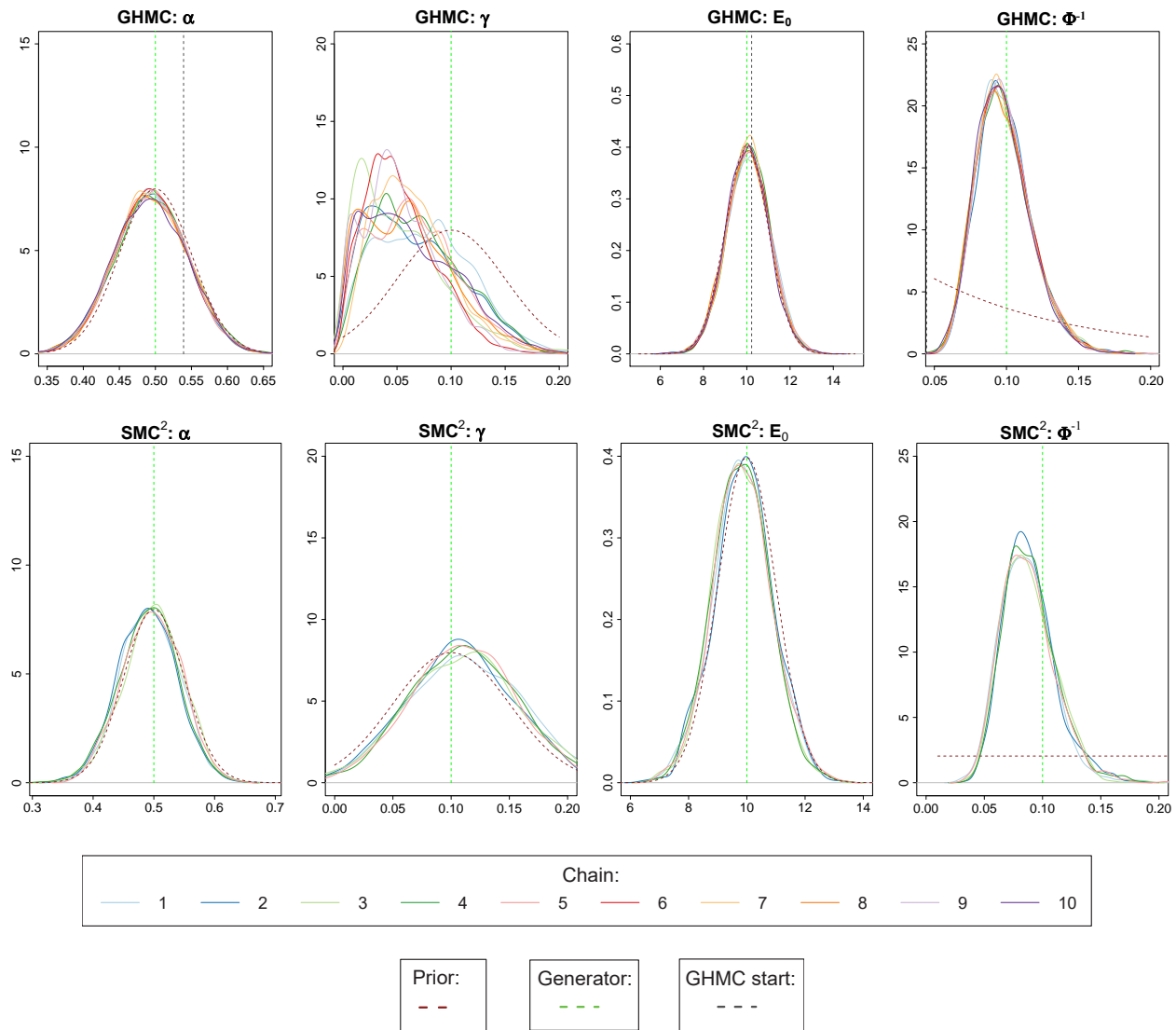


Figure 18: For the synthetic data: parameters' posterior densities for GHMC (top row) and SMR² (bottom row) corresponding to bottom-left of Figures 13 and 15 (SEIR model). Dashed green vertical lines correspond to the true values.

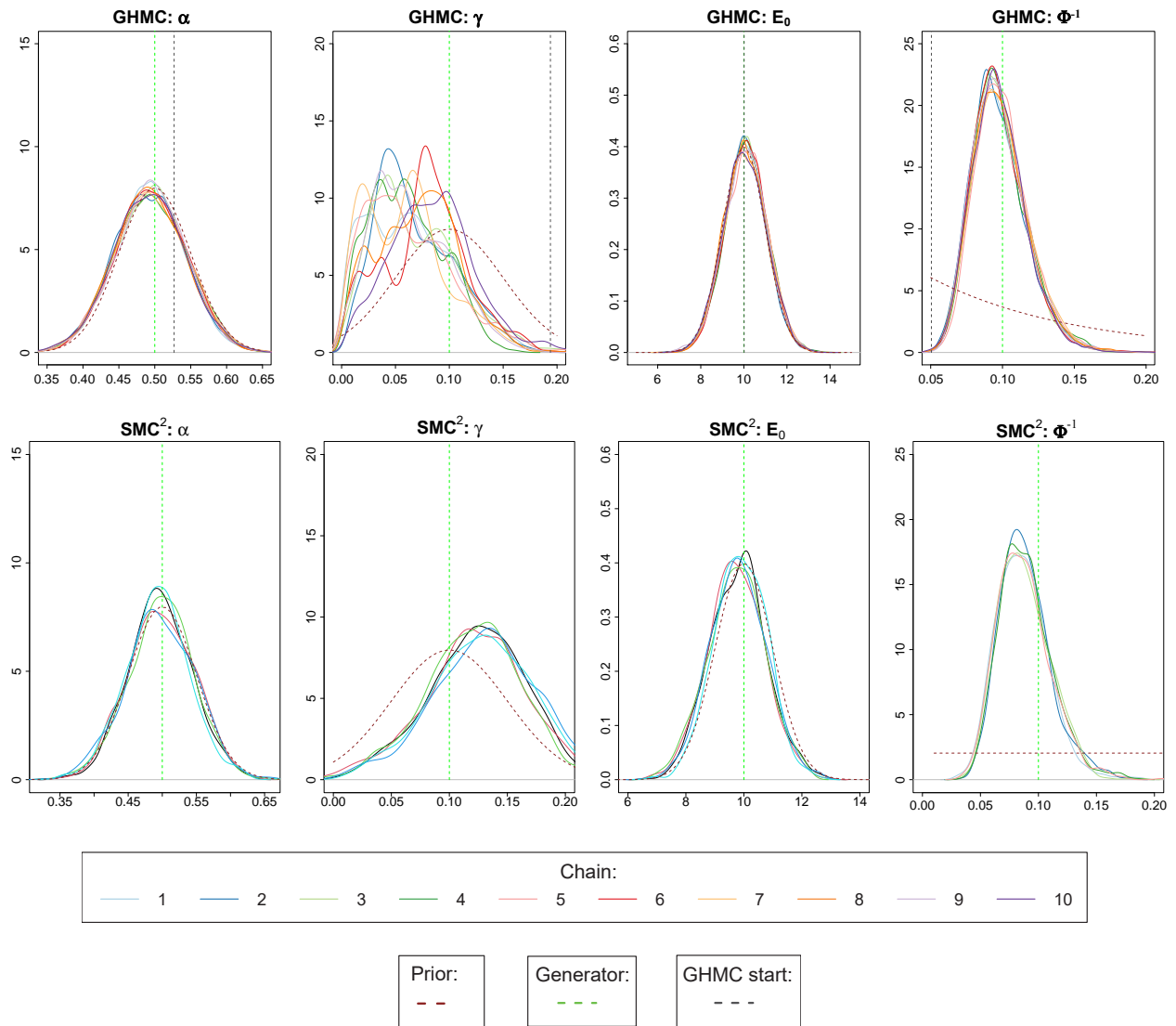


Figure 19: For the synthetic data: parameters' posterior densities for GHMC (top row) and SMR² (bottom row) corresponding to bottom-right of Figures 13 and 15 (SEI₃R model). Dashed green vertical lines correspond to the true values.

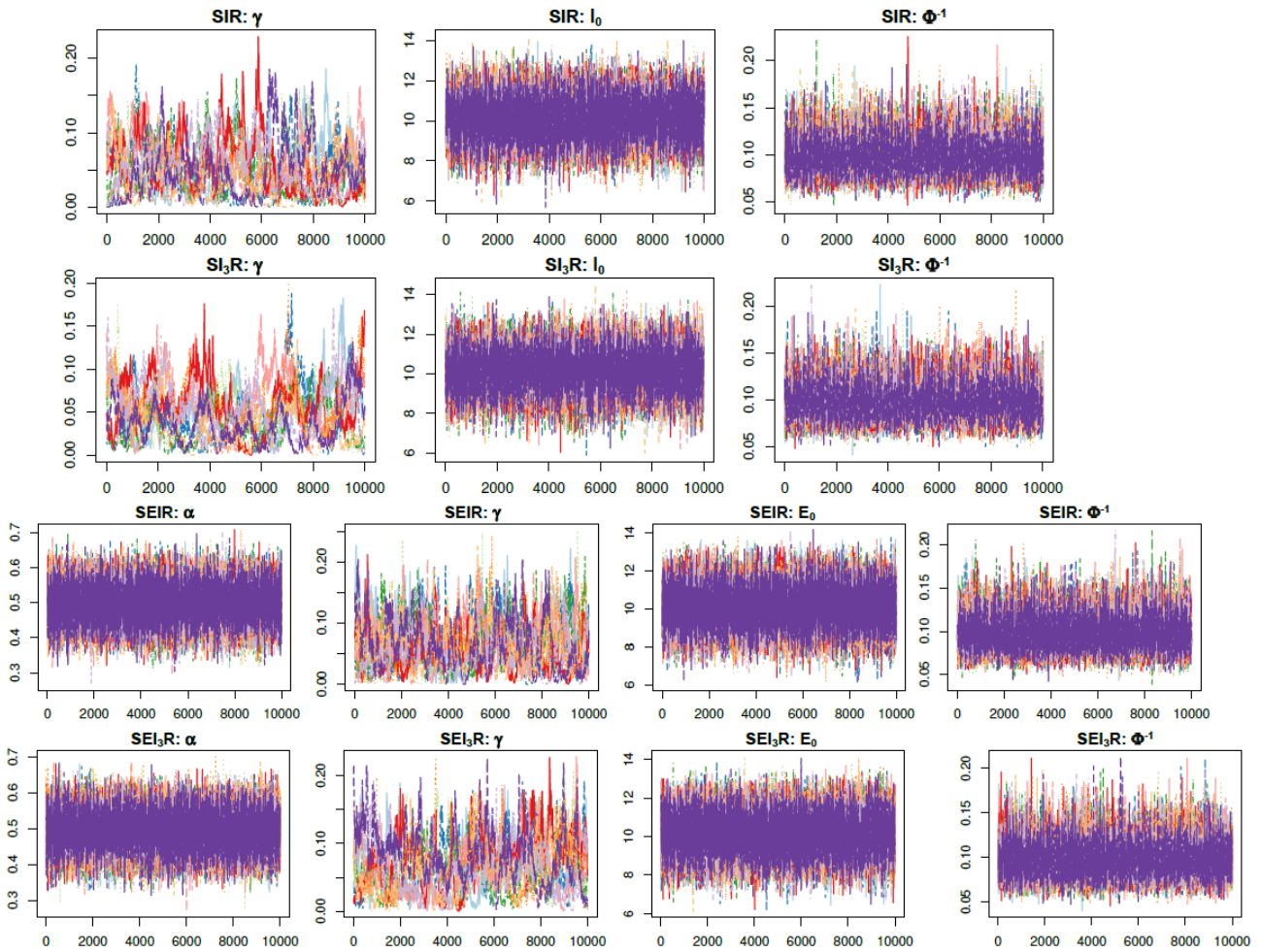


Figure 20: For the synthetic data: trace-plot of the epidemiologically relevant variables for 10 chains of GHMC for the the models corresponding to Figure 13.

E.2 Case study 2: Basque Country data

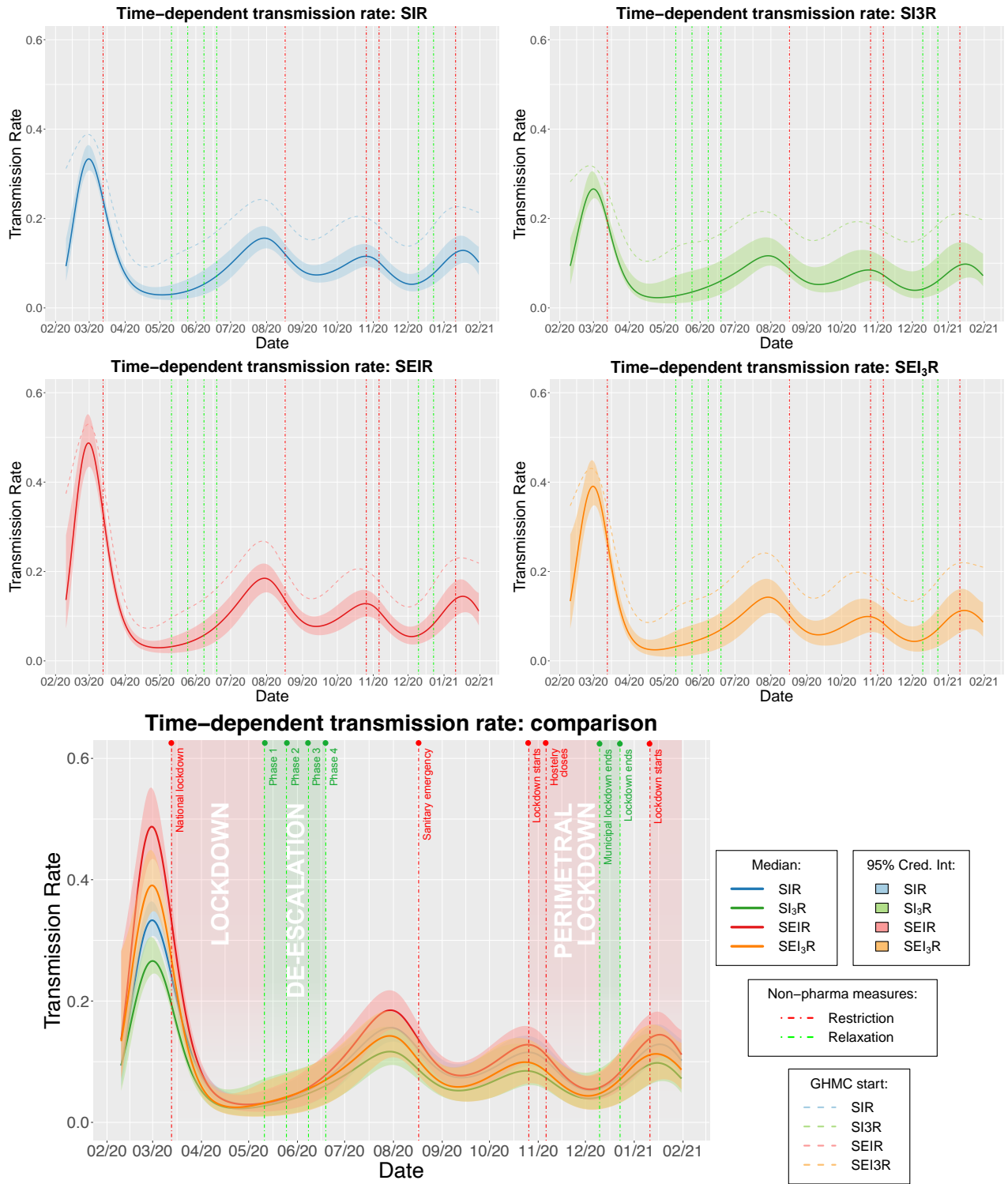


Figure 21: For the Basque Country data: posterior medians (solid lines) and 95% credible intervals (shaded areas) of the time-dependent transmission rate, $\beta(t)$, for spline-based dynamic models (2) (or (17)) and (5) in the main text, sampled with GHMC. Results are shown for a combination of 10 chains with 10000 production steps. Four different compartmental models SIR, SI₃R, SEIR and SEI₃R are displayed. Dashed lines represent the starting values of the chains corresponding to the tuning step in Algorithm 1 in the main text.

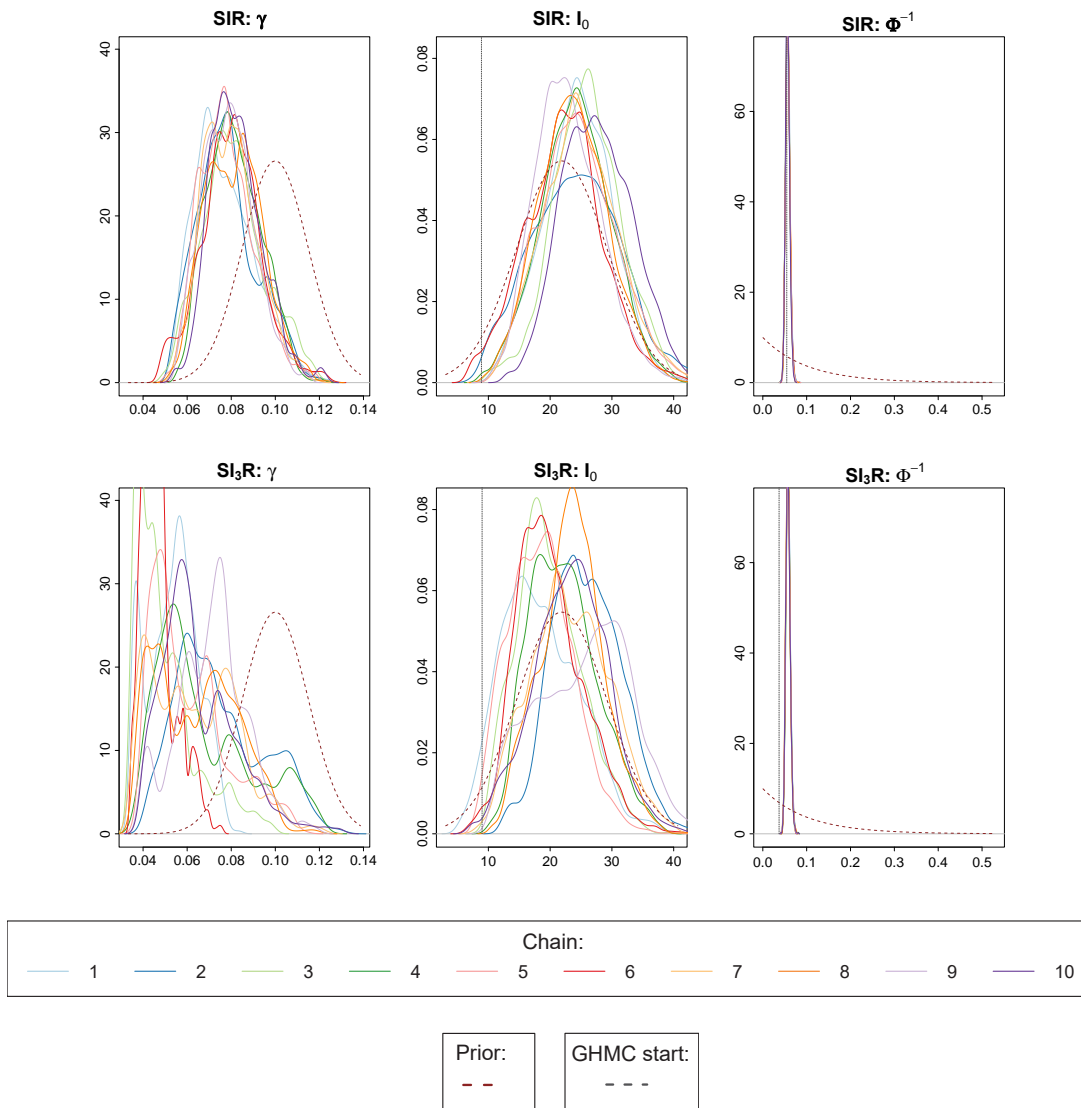


Figure 22: For the Basque Country data: parameters' posterior densities corresponding to 10 chains of GHMC for the SIR and SI₃R models. In dashed brown we have the prior density; in dashed grey we have the initial point of the chains.

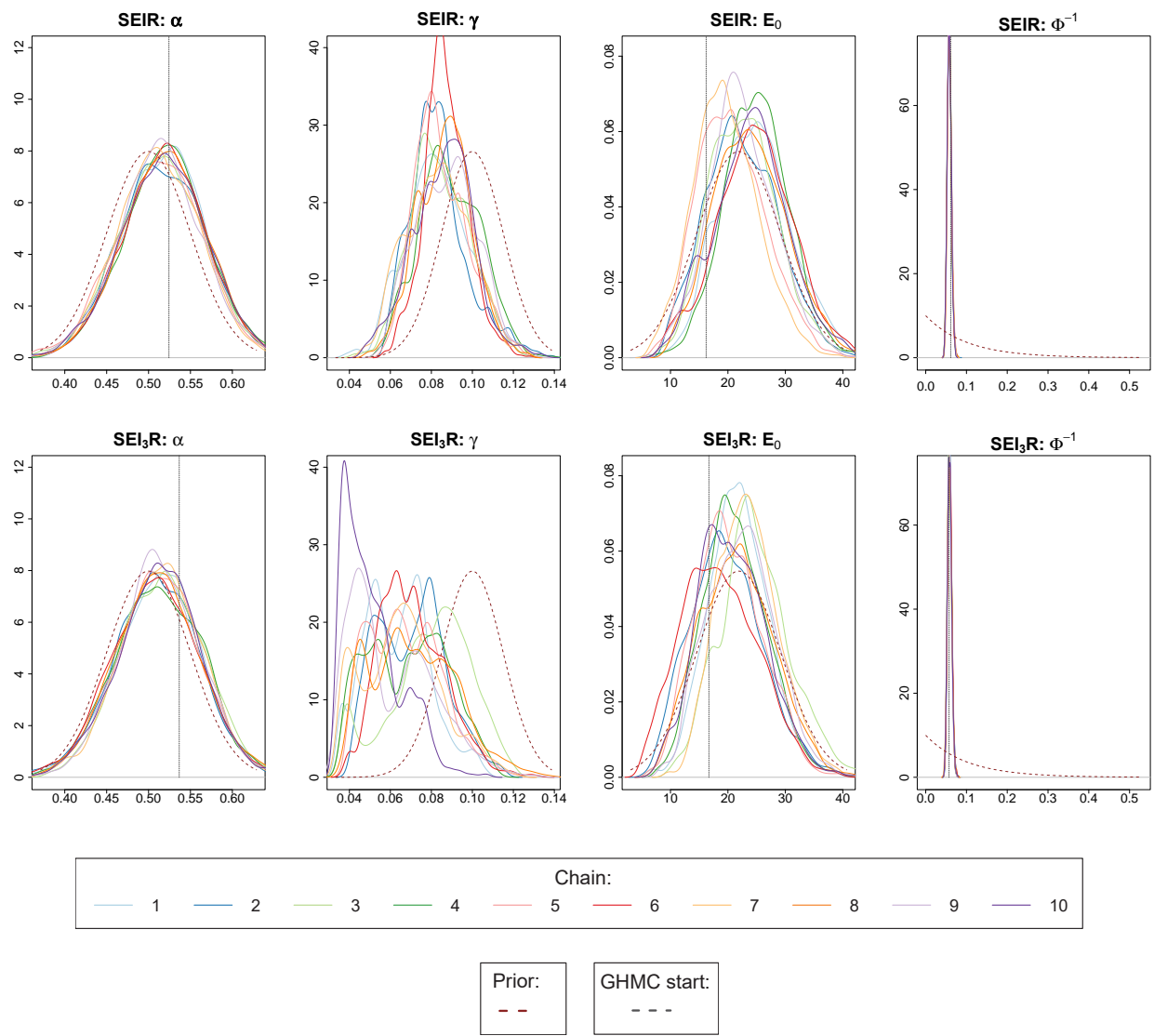


Figure 23: For the Basque Country data: parameters' posterior densities corresponding to 10 chains of GHMC for the SEIR and SEI₃R models. In dashed brown we have the prior density; in dashed grey we have the initial point of the chains.

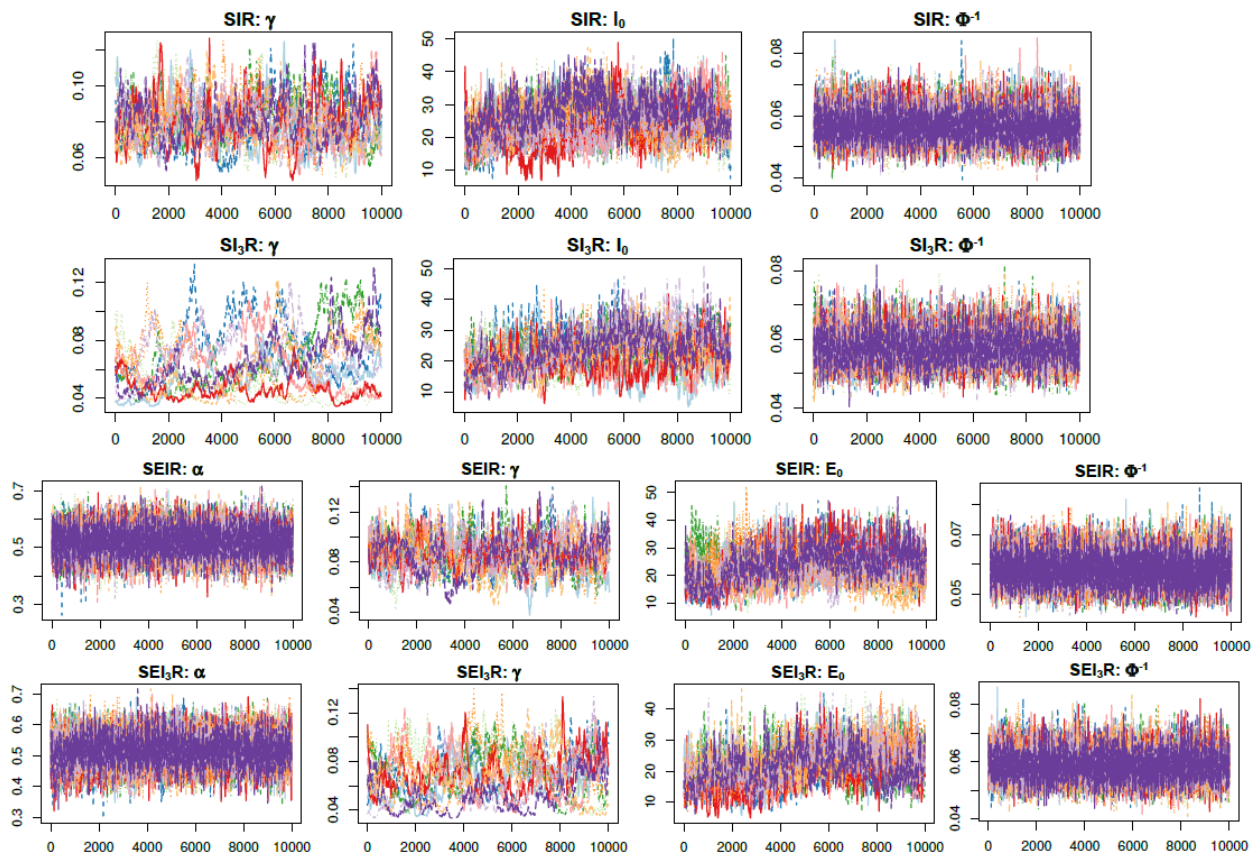


Figure 24: For the Basque Country data: trace-plot of the epidemiologically relevant variables for 10 chains of GHMC for the models corresponding to Figure 5.